Dark Matter Capture by the Sun via Self-Interaction

Author: Axel Widmark

Contact: waxel@student.chalmers.se

Thesis at Master Program Physics and Astronomy
Examiner: Riccardo Catena, Department of Physics

Department of Physics
Chalmers University of Technology
SE-412 96 Gothenburg
Sweden
+46 (0)31-772 10 00

Printed by Chalmers reproservice
Gothenburg, Sweden 2016

MASTER'S THESIS

Dark Matter Capture by the Sun via Self-Interaction

Axel Widmark

Department of Physics
Chalmers University of Technology
Gothenburg, Sweden 2016

Dark Matter Capture by the Sun via Self-Interaction
AXEL WIDMARK
Department of Physics
Chalmers University of Technology

Abstract

There is compelling evidence that dark matter constitutes 85 % of the universe's total matter content. So far, this distinctly different type of particle is observed only in terms of its gravitational effects, but various detection experiments are conducted and underway. One method is indirect detection of neutrinos coming from the Sun. Under the assumption that dark matter consists of Weakly Interacting Massive Particles (WIMPs), one of the most studied dark matter particle candidates, these WIMPs would interact with atomic nuclei within the Sun and be trapped in its gravitational field. After a large enough concentration of trapped WIMPs has been amassed, they would begin annihilating with each other, producing a high-energy neutrino signal. In this thesis I study the possibility that WIMP self-interaction has a significant effect on the total capture rate and resulting neutrino signal. Potentially, an amassed concentration of WIMPs inside the Sun can itself constitute a scattering target and contribute to further captures from the galactic dark matter halo. In order to describe the kinematics of particle interaction and WIMP capture I utilize an effective field theory in the non-relativistic limit. This allows me to explore, in a model-independent way, the parameter space of interaction and the possibility for WIMP capture enhancement due to self-interaction. Upper limits to the strength of these interactions come from direct detection experiments and galaxy cluster observation and simulation. It is found that self-interaction could play a significant role in amplifying the neutrino signal; even an amplification of several orders of magnitude is not ruled out by current limits.

Keywords: dark matter theory, dark matter indirect detection, dark matter self-interaction, WIMP annihilation

Contents

1

Introduction

For many decades now, dark matter has been one of the main concerns of astronomy, particle physics, and cosmology. There is convincing evidence for an abundant and very weakly interacting particle that constitutes about 85 % of all matter and is of paramount importance to the expansion and structure formation of the universe. This elusive particle is hitherto undiscovered and only seen in terms of its gravitational effects, which is why the scientific community calls it *dark matter*. There are a number of competing theories about what this dark matter could be and what phenomenological attributes it might have.

The search for dark matter is an ambitious and extensive world-wide enterprise, relevant for many different fields of physics. The search is conducted with particle collider experiments, ground-based telescopes and satellites, operating by either direct and indirect detection, all of which are continually pushing the envelope towards next-generation experiments.

One method of indirect detection is the search for a neutrino signal that bears the signature of dark matter annihilation, potentially detectable with a neutrino telescope such as IceCube. The are a number of possible origins for this signal, but the focus of this thesis is on such a signal emanating from the Sun.

Assuming that dark matter can interact via the weak force or some other hitherto unknown force of nature, it would collide with atomic nuclei within the Sun. If dark matter particles lose enough kinetic energy in such a collision they would be bound in orbit. With further collisions, they would eventually thermalize and settle in the Sun's core. As the concentration of trapped dark matter particles builds up, they would start annihilating with eachother and eventually reach an equilibrium state where the rate of capture is equal to the rate of annihilation. The annihilation process would produce decay particles, such as neutrinos. These neutrinos would have an energy that is a fraction of the total dark matter particle mass, meaning they would be discernible from the less energetic neutrino flux created in the Sun's fusion process.

What I am exploring specifically is whether or not it is possible that dark matter self-interaction has a significant effect on the total rate of capture and the resulting neutrino signal. Potentially, an amassed concentration of trapped WIMPs in the Sun's core would itself constitute a scattering target for further capture, hence amplifying the capture rate. This is a topic that has not been very well explored in the literature. One article by Zentner [1] suggests that such an amplification is improbable.

In order to model the relevant interactions, I utilize an effective field theory approach in the non-relativistic limit. There are a total number of 14 non-relativistic leading order quantum operators that govern two-body interaction. This description allows for a model-independent analysis of parameter space; in this manner I remain fairly agnostic about the exact nature of dark matter and only adhere to the limits provided directly from observation.

The total capture and annihilation rates are calculated numerically. The annihilation rate is provided by cosmological arguments for dark matter as a relic from the early universe. The limits to the various interaction coefficients are given by direct detection experiments, and observation and simulation of galaxy clusters. The limits for dark matter self-interaction are far less stringent than for dark matter interaction with atomic nuclei, by around ten orders of magnitude. Dark matter particle models that predict such phenomenology are not very prevalent and only a few articles exist on the subject [2]. It remains a field of research that is yet to be explored.

In this thesis, it is found that dark matter self-interaction can have a significant effect on the neutrino signal coming from dark matter annihilation in the Sun. An amplification to the signal due to dark matter self-interaction can be as high as four orders of magnitude, given current limits.

The thesis is structured as follows. In chapter 2, I briefly present the evidence for dark matter, a selection of dark matter candidate particles, and a list of dark matter detection experiments. In chapter 3, I present the theory relevant for this thesis, which includes analytical derivations of dark matter capture by the Sun, effective field theory, and interaction coefficient limits. In chapter 4, I present the evaluations and results, the different capture and annihilation rates and possible factors of amplification due to dark matter self-interaction. In chapter 5, I discuss the results and compare with previous work on the subject.

2

Dark Matter

In this chapter I present a general overview of dark matter: the evidence supporting its existence, a selection of viable candidate particles, and possible methods of detection. I conclude the chapter with the detection technique that is of relevance for this Master's Thesis.

For more information on the subject of dark matter, see the review by Bertone, Hooper and Silk [3].

2.1 Evidence for dark matter

Ever since the publication of Isaac Newton's *Philosophiae Naturalis Principia Mathematica* in 1687, the properties of gravity has been paramount in understanding, describing and predicting the behaviour of astrophysical objects. The first prediction of a hitherto unseen massive body was made by the astronomers Urbain Le Verrier and John Couch Adams, who studied the orbit of Uranus. Its anomalous orbit led them to believe that there was another massive body in the solar system. They were correct, and 1846 the planet of Neptune was observed.

In modern astronomy and cosmology, the study of astrophysical objects and their motion, as well as the study of gravitational lenses, indicate a more exotic type of matter, which is called dark matter due to its elusive qualities.

A first observation of dark matter was made by the Swiss astronomer Fritz Zwicky in 1933 [4]. He studied the Coma galaxy cluster by means of the virial theorem, which relates a cluster's radius and velocity dispersion to its mass. He found the cluster to be much heavier than expected, with a mass-to-light ratio that was two orders of magnitude higher than that of the solar neighbourhood. He called this elusive unseen mass *dunkle Materie*. Although this discovery was

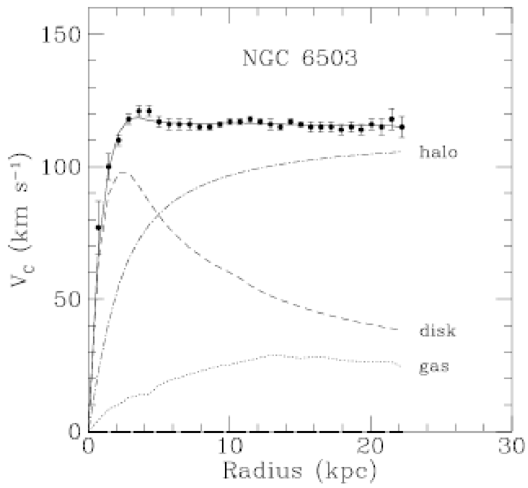

Figure 2.1: The rotational velocity of spiral galaxy NGC6503 [6]. The black dots represent the measured data. The lines correspond to the contributions from gas, disk, and dark matter.

puzzling, it would take many decades before the issue became a prime concern of the scientific community.

Evidence for dark matter has been observed in a vast span of distance scales, ranging from the galactic to the cosmological scale. While an observational anamoly at some scale of distance could be explained in a variety of ways, for example by modifying the force of gravity, all these different observations has not been explained conclusively by any other singular phenomena. This makes the case for the existance of dark matter very convincing.

2.1.1 Galactic scale

In the 1970's the American astronomer Vera Rubin made observations of rotational velocities in spiral galaxies [5]. In a spiral galaxy, the visible baryonic matter density (stars, gas and dust) decreases the further you get from the galactic center, which would infer a decreasing rotational velocity. What Rubin found was that the rotational velocity does not decrease with radius, but rather stays more or less constant in the outer rims of the galaxy, as illustrated in figure 2.1. This came to be called the *galaxy rotation problem*, one of the most convincing pieces of evidence of an unseen, very heavy and fundamentally different type of matter.

The rotational velocity of a spiral galaxy holds information about the dark matter halo density and shape. While there is not much discussion about the halo distribution at large radii, its shape at short radii is still under debate. N-body simulations of *collisionless* dark matter exhibit a very steep halo shape, with high halo density in the galactic core [7]. Observations, on the other hand, point in the other direction, of a more shallow or even flat halo profile [8]. This is highly relevant for this Master's Thesis, as it could suggest that dark matter particles are in fact *not* collisionless, but interact with sufficient strength to affect the shape of galactic dark matter halos [9][10]. However, it is under debate if this could instead be explained by energy dissipation through supernova explosions [11], so no consesus has been reached so far. See section 3.3 for further discussion and estimates of the strength of dark matter self-interaction.

There is yet other evidence for dark matter coming from kinematic arguments, from the velocity dispersion of stars in spheroidal dwarf galaxies [12], or the motion of spiral galaxy satellites [13].

Gravitational lensing is another useful tool for providing proof of dark matter. In fact, it is the only way to make direct mass measurements of a galaxy (as opposed to the kinematic methods previously mentioned). Gravity manifests itself as a curvature of space-time, as described by Einstein's general relativity, so that light is bent in a strong gravitational field. This phenomena is most dramatic when two galaxies are in the same line-of-sight, what is known as *strong gravitational lensing*. The foreground galaxy will act as lens with respect to the light coming from the background galaxy, whose image will be bent into an arc, as can be seen in figure 2.2. The size and curvature of this arc, and the distances involved, are directly linked to the mass of the lensing foreground galaxy. While this provides a very direct tool of analysis, less dramatic effects can also be analyzed by statistical means. The image of a background galaxy under *weak gravitational lensing* will only be slight thwarted, but a large enough data set of thwarted images will still be indicative of the foreground mass distribution. This principle is applied to deep and wide galaxy surveys, which provides evidence for the large-scale structure of matter in the universe and constraints on cosmological parameters [14].

2.1.2 Galaxy cluster scale

As mentioned in the beginning of this section, the very first observation of dark matter is on the scale of galaxy clusters, coming from Fritz Zwicky's study of the Coma cluster. This is the same type of kinematic method used on the galactic scale. In the same vein, the mass measurement method of gravitational lensing used on the galactic scale are also applied to galaxy clusters.

A technique that is unique for galaxy clusters, however, is the study of X-ray emission from intergalactic gas [15]. Galaxy clusters are enormous structures and that attract large amounts of material. Intergalactic gas, mainly hydrogen, falls towards the gravitational center of these clusters and create a superheated plasma

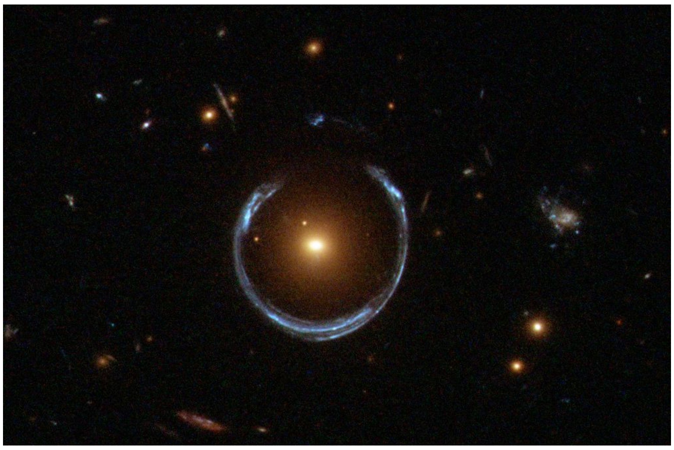

Figure 2.2: A case of strong gravitional lensing, from the Hubble Space Telescope. The yellow foreground galaxy acts as a lens, distorting the image of the blue background galaxy almost into a full circle. The image is taken from Wikimedia Commons.

in the temperature range of 10^7–10^8 K. This gas emits X-rays, from which it is possible to estimate the gravitational strength and total mass of a cluster. This technique shows that there must be significantly more matter in between galaxies than in the galaxies themselves, matter that is not visible.

A very compelling piece of evidence for dark matter is the notorious Bullet Cluster [16]. It is visible in figure 2.3. It consists of two galaxy cluster that have passed through each other, so that the gas constituent of the clusters have collided and been trapped in between the clusters, while the stars and dark matter has continued in their respective path without being hindered by the collision. This observation very convincingly shows that the mass of the clusters largely consists of some very weakly interacting mass distribution in a halo-like configuration. The Bullet Cluster is of great relevance for this thesis, as it places upper limits on the strength of dark matter self-interaction, which will be discussed further in section 3.3.

2.1.3 Cosmological scale

In order to account for the cosmological arguments and evidence for dark matter, I first give a very brief overview of the key concepts of mainstream cosmology, of a Big Bang and ΛCDM universe, often referred to as Standard Cosmology.

The fundament of cosmology comes from Einstein's equations,

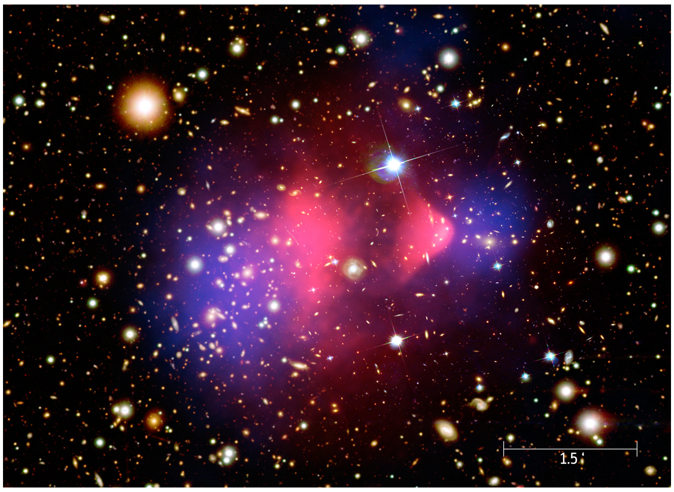

Figure 2.3: The Bullet Cluster, in a composite image with optical light from Magellan and Hubble Space Telescope and X-ray light from Chandra X-ray Observatory. The X-ray emission is represented in pink. The clusters' mass distribution is represented in blue, calculated by means of weak gravitational lensing. The image is taken from Wikimedia Commons.

$$R_{\mu\nu} - \frac{1}{2} g_{\mu\nu} R = -\frac{8\pi G}{c^4} T_{\mu\nu} + \Lambda g_{\mu\nu}, \tag{2.1.1}$$

where $R_{\mu\nu}$ and R are the Ricci tensor and scalar that describe the curvature of spacetime, $g_{\mu\nu}$ is the spacetime metric, $T_{\mu\nu}$ is the stress tensor, which accounts for energy and mass densities, Λ is the cosmological constant, G is the gravitational constant, and c is the speed of light. The left-hand side of the equation represent the geometry of the universe, the curvature of spacetime, while the right-hand side represents the energy content of the universe. The mysterious cosmological constant, Λ, represents a vacuum energy, an energy of space itself. It was first introduced by Einstein in an attempt to model a steady-state universe, but he subsequently abondoned the idea when it became clear from observation that the universe is in fact expanding. The story does not end there, however, as it was discovered that the universe is not only expanding but also expanding faster and faster. This observation prompted the cosmological constant to be reintroduced. Today, the vacuum energy represented by Λ in Einstein's equations is commonly referred to as *dark energy*.

Under assumptions of a homogenous and isotropic universe, which is well supported by observation at scales larger than ~ 100 Mpc, Einstein's equations take a rather simple form. This leads to what is known as the Friedmann equations, that describe the expansion of the universe. The two independent Friedmann equations are

$$\left(\frac{\dot{a}}{a}\right)^2 + \frac{kc^2}{a^2} = \frac{8\pi G}{3}\rho + \frac{\Lambda}{3} \tag{2.1.2}$$

$$\frac{\ddot{a}}{a} = -\frac{4\pi G}{3}(\rho + \frac{3p}{c^2}) + \frac{\Lambda}{3}, \tag{2.1.3}$$

where a is the scale factor or "radius" of the universe, $\dot{a}$ refers to its derivative in time, ρ is the matter density, p is pressure, and k is the spatial curvature of the universe. The quantity k can take values -1, 0, or 1, which corresponds to an open, flat, or closed geometry.

The quantity $\dot{a}/a$ is more commonly known as the Hubble parameter, denoted H. The Hubble constant, H_0, is the Hubble parameter at present time and the current rate of expansion in the universe. It has value $H_0 = 67.8 \pm 0.9$ km s^{-1} Mpc^{-1} [17][18].

The different energy densities of the universe are differently affected, or thinned out, by its expansion. For example, the matter density is inversely proportional to the volume of the universe, while the vacuum energy density does not scale at all but remains constant. Thereby the expansion of the universe is contingent on the distribution between species of energy; which type of energy density that is the dominant driving force of expansion can change over time. A canonical definition is that of abundances,

$$\Omega_i \equiv \frac{\rho_i}{\rho_c}, \tag{2.1.4}$$

where the subindex i can represent matter, radiation, vacuum energy, or spatial curvature. The quantity ρ_c is the critical density, the total current energy density (including vacuum energy) that with observational value for H_0 would infer a geometrically flat universe. Expressed in terms of redshift, z, the expansion rate can be written

$$\frac{H^2(z)}{H_0^2} = \Omega_\Lambda + \Omega_k(1+z)^2 + \Omega_M(1+z)^3 + \Omega_R^2(1+z)^4. \tag{2.1.5}$$

The second term on the right-hand side, with abundance Ω_k, comes from the spatial curvature and is zero in a flat universe.

The universe used to be hotter and denser and particles that today are not interacting very strongly was once in thermal equilibrium. The governing equation is the Boltzmann equation,

$$\frac{dn}{dt} + 3Hn = -\langle\sigma_A v\rangle(n^2 - n_{eq}^2), \tag{2.1.6}$$

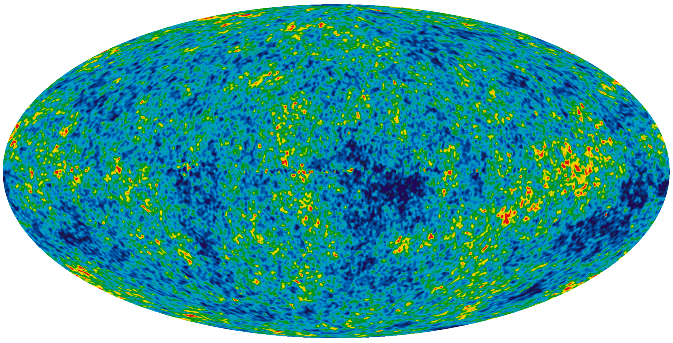

Figure 2.4: A map of CMB temperature fluctuations on the sky, from the WMAP survey. The image is taken from Wikimedia Commons.

where n is the number density, n_{eq} is the number density at thermal equilibrium, and $\langle \sigma_A v \rangle$ is the thermally averaged annihilation cross section. At some point in time, the expansion rate of the universe became dominant with respect to the interaction rate of the particle. In other words, the term proportional to the Hubble parameter grew larger than the interaction term on the right-hand side, and the equilibrium state was lost. The particle species is said to be *decoupled* or experience a *freeze-out*, which is hypothesized to have happened to dark matter (at least for most dark matter particle candidates).

A similar, although not completely analogous, example of a decoupling is the cosmic microwave background (CMB). This decoupling was due to a drastic change in the density of charged scattering targets. As the universe cooled enough for neutral atoms to form, space became permeable for light, resulting in the decoupling of photons. The CMB is the last scattering surface of the plasma state of the universe, a remnant from around 370,000 years after the Big Bang.

While the CMB is direct evidence of the Big Bang theory, it also provides constraints for cosmological parameters and determines the total amount of dark matter in the universe. The CMB is a black body spectrum of temperature 2.726 K, to an accuracy of 10^{-5} in all directions. Below this level of accuracy, however, there are temperature fluctuations, which have been measured in surveys like Cosmic Background Explorer (COBE), Wilkinson Microwave Anisotropy Probe (WMAP), and Planck Satellite. A map of these fluctuations can be seen in figure 2.4.

Expanding the CMB into spherical harmonics gives a power spectrum, which charts the angular scale of the fluctuations, see figure 2.5. This power spectrum sets strong limitations on the underlying cosmological parameters. Coupled with power spectrums of visible matter, these constraints can be made even stronger. Estimates of the cosmological parameters in the Standard Cosmology framework, using data from the Planck Satellite, suggest a present energy distribution of ~ 69

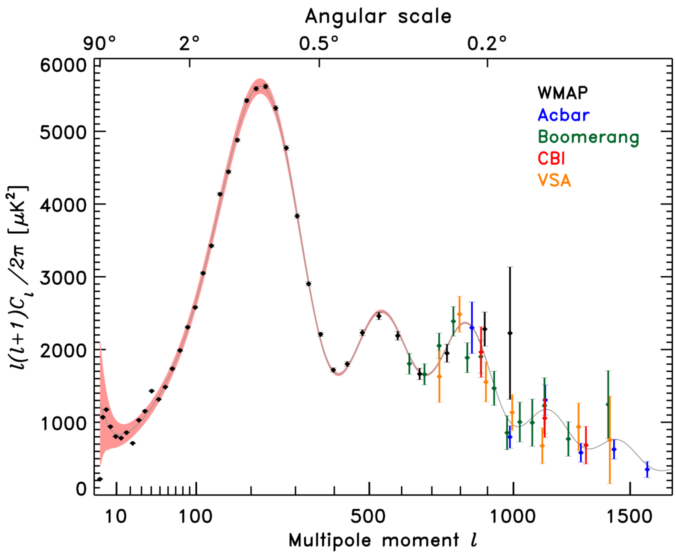

Figure 2.5: CMB power spectrum, with data from various surveys. The lower horizontal axis shows the multipole moment, l, of the spherical harmonics functions. The image is taken from Wikimedia Commons.

% dark energy, $\sim$ 26 % dark matter, and $\sim$ 5 % ordinary baryonic matter [17][18].

2.2 Dark matter candidates

There are a great number of dark matter candidate particles, some of which are considered more promising than others. In this section I present a select few of the most prominent candidates, including the subset of particular relevance for this thesis. Note that there is no requirement for dark matter to consist of a single particle species.

Sterile neutrino

At first glance, Standard Model neutrinos fulfill a lot of the qualifications of a dark matter candidate; they have mass and are weakly interacting. However, given their relic density, they are not massive enough to significantly contribute to the total amount of dark matter in the universe. Furthermore, their low rate of interaction and low mass correspond to a long free streaming length [19], meaning that they could not account for the structure formation on scales below $\sim$ 40 Mpc. Therefore Standard Model neutrinos are excluded. However, neutrinos that are *sterile*, meaning that they do not interact via the weak force, with mass of at least

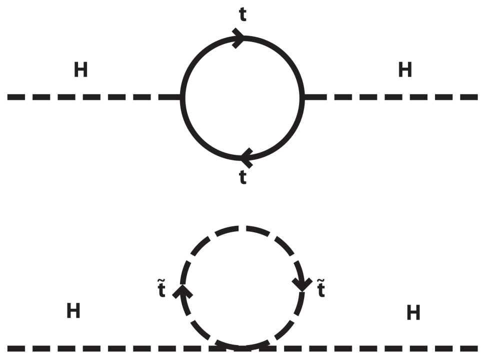

Figure 2.6: Loop diagrams to illustrates the hierarchy problem. The top diagram represents the first-order loop correction to the Higgs mass, coming from the top quark. The bottom diagram represents the loop correction coming from the top quark's superpartner, the stop quark. The image is taken from Wikimedia Commons.

~ 10 keV, have been proposed as a candidate [20].

Axion

The *axion* was introduced in an attempt to solve the CP-problem of particle physics. The CP-problem is the puzzling question about why it is that quantum chromodynamics seems to uphold CP-symmetry. There is not *a priori* reason as to why it should, but the existance of the axion would explain it. Constraints coming from laboratory detection attempts and astrophysical arguments tells us that the axion must be very light, in the range of 0.01 eV or lower. The calculation of the axion relic is uncertain, but it possible to find a set of parameters that are in accordance with present-day cosmological constraints [21].

Supersymmetric candidates

Supersymmetry (SUSY) is an extension of the Standard Model of particle physics [3][22][23]. It relates the fermionic fields (also known as matter fields) to the bosonic fields (force-carrying fields). In SUSY theory, the particles of the Standard Model have supersymmetric partner particles, sharing all quantum numbers except spin that differs by a half-integer.

While the symmetry itself has an appealing quality of unification between matter and interaction, it also presents a solution to a very significant conundrum known as the *hierarchy problem*. The hierarchy problem concerns a remarkable fine-tuning of natural parameters, arising from the radiative corrections to the mass of the Higgs boson. This mass correction comes from a loop diagram, as seen in figure 2.6. In the top diagram of the figure, a top quark loop affects the free propagation of the Higgs boson, giving it a quadratic mass correction of order

$$\delta m_H^2 \sim \Lambda_{UV}^2, \tag{2.2.1}$$

where Λ_{UV} is the ultraviolet cutoff, the energy scale at which new physics comes into play and the Standard Model breaks down. If this cutoff happens at Planck scale, then the natural expectation would be for the Higgs mass to have a value close to this cutoff scale, something like $\sim 10^{18}$ GeV. However, the Higgs boson mass is measured to be 125 GeV. These numbers are of vastly different order of magnitude, which suggests a remarkably improbable fine-tuning of parameters, such that the intrinsic mass of the Higgs boson cancels to an extreme precision with the radiative mass corrections. This is the essence of the hierarchy problem.

A possible solution comes from SUSY, which postulates the existance of superpartner particles. The top quark would have a superpartner called the *stop quark*. The stop quark would in turn give rise to its own loop correction, as seen as the bottom diagram in figure 2.6. The top and stop quark corrections would have different signs, and so their combined mass correction would be

$$\delta m_H^2 \sim ({m_t}^2 - {m_{\tilde{t}}}^2). \tag{2.2.2}$$

In this case, the mass of the Higgs boson and its loop diagram correction would be of roughly the same order of magnitude, which would nullify the issue of fine-tuning.

Various superpartner particles have been proposed as dark matter candidates. The type of particle called *neutralino* is one of the most studied of all dark matter particle candidates. In SUSY, there are neutral superpartners to the B and W_3 gauge boson, called bino and wino, and to the H_1^0 and H_2^0 Higgs bosons, called higgsinos. Together, these superpartner states mix into four fermionic neutralino mass states. It is hypothesized that these neutralinos would adhere to a so-called R-symmetry, meaning that any creating or annihilation event involves an even number of superparticles. This symmetry is necessary in order for the theory to exclude events like proton decay. In effect, only the lightest neutralino is stable and the production of a heavier neutralino would result in a cascade of decays into the stable state.

There are other, perhaps less favored, superpartner particles that are considered to be dark matter candidates. The *sneutrino* is the superpartner to the neutrino, speculated as a viable dark matter particle in the TeV mass range. The *gravitino*, superpartner to the graviton, is backed by strong theoretical motivations. However, it would be very difficult to detect, as it only interacts via gravitational force. The *axino*, superpartner to the hypothesized axion mentioned above, is plausible, even as a cold dark matter candidate if generated through some process outside thermal equilibrium.

Kaluza-Klein states

There are exotic dark matter candidates that arise in models of extra dimensions. Although we see a 4-dimensional spacetime, the universe could potentially be higher dimensional, with additional dimensions visible at high energy or short distance. This has some interesting theoretical ramifications such as the unification of forces, introduced as a concept by Kaluza in 1921 when he unified electromagnetism and gravity in a 5-dimensional theory. It could also explain the discrepancy of strength between the weak force and gravity. Furthermore, a higher-dimensional spacetime is hypothesized in string theory and M-theory, with a total number of 10 or 11 dimensions. These theories could constitute a description of quantum gravity and a unified theory of all interaction.

As it happens this theory also give rise to a potential dark matter candidate. The additional spatial dimensions could be *compactified*, meaning that they are finite and probably very small. The simplest case would be that a compactified dimension is in the shape of a circle. In such a circle, the momentum travelling through it would be quantized. While Standard Model physics would exist the lowest state, with no momentum going in the direction of the compactified dimension, there would exist a possibility of excitations, holding a ladder of excited *Kaluza-Klein states*. This would correspond to additional particles outside the Standard Model, and potentially a dark matter particle [24].

Wimpzilla

There are theories of superheavy dark matter candidates, often referred to as *wimpzillas*. While most candidate are in the range of a hundred or a thousand GeV, wimpzillas are hypothesized to have a mass larger than 10^{10} GeV. Dark matter particles of high mass can be ruled out as thermal relics from the early universe, as the freeze-out from thermal equilibrium for such a particle is not in accordance with constraints from the CMB. (See section 2.1.3 for the theory behind such considerations.) Superheavy wimpzillas, however, need not have been in thermal equilibrium at all during freeze-out, so their relic abundance does not depend on their annihilation cross-section.

An argument for the existance of wimpzillas is the observation of ultra-high energy cosmic rays, well above the GZK cutoff at $\sim 5 \cdot 10^{10}$ GeV. This cutoff is the energy at which cosmic rays can scatter against the CMB, thus hindering the propagation of such a cosmic ray [25]. The astrophysical origin of such cosmic rays is unclear, but perhaps it comes from the annihilation of superheavy particles such as the wimpzilla [26].

Miscellaneous candidates

There are a number of various candidate particles, far too many to account for in detail. A *scalar particle* have been proposed in different contexts as a dark matter candidate, for example in what is called the Little Higgs model. There is also *Q-balls*, *charged massive particles* (*CHAMPs*), *mirror particles*, *fourth generation neutrinos*, etcetera [3].

2.2.1 WIMP

The term Weakly Interacting Massive Particle, WIMP, refers to all candidate particles that are just that, weakly interacting and massive, typically around 100 GeV. For example, the SUSY candidates discussed above would fit into this category, as well as the Kaluza-Klein particles or heavier neutrinos.

The WIMP density would be a thermal relic from the early universe. The WIMPs would have experienced a freeze-out when the universe expanded and cooled, such that the weak force interaction could no longer keep the WIMPs in thermal equilibrium with other particle species. (See the discussion in section 2.1.3 for the theory behind these statements.) Given the present abundance of dark matter, these considerations predict a WIMP self-annihilation cross-section of $\langle \sigma_A v \rangle \simeq 2 \cdot 10^{-26}$ cm^{3}s^{-1} in the relevant mass regime [27].

In this thesis, the dominant dark matter constituent will be assumed to be WIMPs, and referred to as such. Other than that I assume for the WIMPs to be in the mass range of 10–1000 GeV, and with spin 1/2.

2.3 Dark matter detection

In this section I present the various strategies of dark matter detection. I will conclude this section and chapter with the detection strategy that is in focus for this thesis, namely that of a neutrino signal produced by an annihilation of WIMPs in the Sun's core.

2.3.1 Collider searches

If the dark matter particle mass is of an energy scale reachable for a particle collider, that dark matter particle could potentially be produced inside the collider.

Because dark matter interactions with baryonic matter are so weak, the produced dark matter particle would simply escape the collider without being detected, much like neutrinos do. This would leave a signature trace of lost energy and momentum.

Such searches have provided strong constraints on the dark matter candidate particles, but are often model dependent. A majority of such searches focus on a SUSY model and the production of some type of neutralino, a candidate particle presented in section 2.2. In such a model, only the lightest neutralino is stable. The production of heavier neutralinos would result in a cascade of decays, producing lepton and/or quark jets that could be detected. Such a signal has been looked for at the Large Hadron Collider (LHC) at CERN.

Conversely, model-independent analysis is also performed, by means of effective field theory (EFT), which will be discussed thoroughly in section 3.2. The EFT approach analyses the parameter space of all possible interaction operators in the limit of low momentum transfer, without model-dependent bias towards what the interaction should look like. Collider data, for example from the LHC, provide constraints on this parameter space. However, applying this low-energy or low-momentum limit analysis for collider experiments can be problematic, as dark matter interactions with Standard Model particles might be dominated by behavior outside the parameter region of the EFT [28].

For further information on collider searches for dark matter, see reviews by Bertone *et al.* [3] and Klasen, Pohl and Sigl [29].

2.3.2 Direct detection

Direct detection of dark matter is very straight forward, at least conceptually. If the galaxy contains a distribution of WIMPs that our solar system travels through, then WIMPs would sporadically interact with the baryonic matter of the Earth. A detector could measure the effects of such interactions happening inside it, typically by recording the recoil energy of atomic nuclei as produced by a WIMP-nucleus collisions.

In the past few years, direct detection sensetivity has improved tremendously. Even so, no direct detection has been recorded, or at least not conclusively proven. On the other hand, direct detection experiments have provided strong limits for WIMP-nuclei elastic scattering cross-sections.

A WIMP detector faces a number of challanges. It must be sensitive to very small energies imparted by the interaction of a WIMP, while at the same time minimizing the background signal. It must also have a large enough detector mass, thus constituting a large target volume for passing WIMPs. In the same vein, the detector must have acceptable performace over a long time, preferably a few years, for detection to be statistically feasable. Below I present the various direct detection techniques being utilized.

For a more extensive review on the subject of dark matter direct detection, see review by Undagoitia and Rauch [30].

Noble-gas detector

This type of detector, constructed as a container with liquid noble-gas, constitutes a large and homogenous target. The most common detector media are xenon and argon. A deposit of recoil energy in the noble gas causes excitation or ionisation. This can lead to formation of excimers, which are short-lived molecular structures between ionised noble-gases. A recombination into ground-state emits ultraviolet photons which can be detected. Free electrons that are produced in ionisation can be extracted by applying an external electric field to the detector, enabling analysis of this additional signal. The sought after signal can be distinguished from the background signal, coming mainly from electron and gamma ray recoils, by measuring and comparing the emitted ultraviolet light and the rate of ionisation.

Examples of such experiments are the series of ZEPLIN detectors [31] in the UK or the XENON detectors [32] at Gran Sasso, Italy. An experiment called LUX [33], installed at the Sanford Underground Laboratory, started collecting data in 2013. Since then, it has improved on previous limits for the WIMP-nuclei interaction strength. These are the limits used in this thesis. For further information, see section 3.3.

Scintillator crystal

Scintillators are among the most common detection devices in particle physics. A scintillator material has the property of luminescence, meaning that it emits light when excited. A WIMP collision inside the crystal would deposit energy, subsequently emitted as photons that can be measured. The most common dark matter detector materials are NaI and CsI crystals. An advantage of this technique is its simplicity and sturdiness, enabling a detector to operate for several years.

An example of a NaI crystal detector is the DAMA expreriment [34] at the LNGS underground laboratory in Gran Sasso, Italy. The DAMA experiment has shown some controversial results. It has measured a signal with annual modulation in the energy range of 2–6 keV, over a total of 14 years [35]. An interpretation is that the signal comes from WIMP-nuclei collisions, with an annual modulation due to that the Earth moves through the dark matter halo medium with different speeds at different times of year. However, this modulation signal could be due to other effects, like atmospheric muons, which could follow a pattern of annual modulation. Other experiments, like KIMs at the Yangyang laboratory in Korea, does not support the results of DAMA [36].

Germanium detector

A germanium detector is a semi-conductor that measures a deposit of energy by the resulting electron-hole pairs that are formed. These free charges are carried by an electric field to their corresponding electrodes and detected. The rise-time of such an electrical signal can be used to exclude background events. The noise level is reduced sufficiently by cooling the device to the temperature of liquid nitrogen, 77 K, which bypasses the need for expensive cooling techniques. The threshold for a detectable energy deposit is very low, down to ~ 0.5 keV, allowing searches for WIMPs with mass of only a few GeV.

The CoGeNT experiment [37] at the Soudan Underground Laboratory in the United States is an example of such a detector. It has been collecting data since 2009.

Cryogenic bolometer

A cryogenic bolometer is a crystal detector sensitive to phonons (vibrations of the crystal lattice). In order to reduce the background noise, the crystal must be cooled to a temperature of 10–100 mK. The set-up allows for distinctions between a minimal but measurable rise in temperature and more long-lived athermal phonons. The latter can be used to directly measure both location and magnitude of a deposited recoil energy from a WIMP-nuclei or even a WIMP-electron collision. Combined measurements of different types of signal can be used to exclude background events. By applying an external electrical field to the crystal, a formed electron-hole pair can be caused to drift, producing more phonons. With this technique, the energy sensitivity threshold can be lowered.

Examples of such detectors are SuperCDMS [38] in the United States or EDELWEISS [39] in France.

Superheated fluid

This type of detectors consist of a superheated fluid, meaning that the fluid is kept in a temperature that is above its boiling point. A deposit of energy in this medium induces a phase transition and creates a bubble. The size of such bubbles reveals the magnitude and localization of the energy deposited. After such a bubble is formed, the fluid is compressed and decompressed in order to recover the superheated state. A major advantage of this technology is that its low sensitive to ionisation backgrounds, which dominates the background signal of other dark matter detectors.

Examples of such experiments are COUPP [40] in the US, PICO [41] in Canada, and SIMPLE [42] in France.

Directional detector

A directional detector exploits the direction of the recoil momentum, to see if there is an over-representation in accordance with the expected flow of WIMPs relative to the Earth. An assymmetry in the scattering events could be caused by this “wind” of the dark matter halo. Current directional detectors utilizes a gas container and measures the drift of charged particles in it.

DRIFT-II [43] is currently the largest directional detector, operated at the Boulby Underground Laboratory in the UK.

2.3.3 Indirect detection

Indirect detection of dark matter seeks to measure radiation or particles that are products of dark matter annihilation and decay, typically with a signature energy level that is some fraction of the dark matter particle mass.

For a more extensive review on the subject, see review by Gaskins [44].

Gamma ray detection

Highly energetic photons would be an excellent signal coming from WIMP annihilation. A gamma ray signal permits very exact analysis, both of its energy and its direction of origin.

Because high-energy photons interact in the atmosphere to form electron-positron pairs, direct detection of gamma rays is only possible from space. Traces of gamma rays are still visible from Earth by studying the rest products of gamma rays entering the atmophere. A highly energetic muon or electron can be detected by measuring the Cherenkov light, which is a sort of “sonic burst” but for light, created when a charged particle travels through a medium faster than the speed of light propagation in that medium. Such a detector is the High Energy Stereoscopic System (HESS) [45] in Namibia, which has been running since 2003. Another is the High-Altitude Water Cherenkov Observatory (HAWC) [46] in Mexico, which has been collecting data since 2014. It is sensitive to high-energy gamma rays above 100 GeV.

An example of a gamma ray detector in space is the Fermi Large Area Telescope (LAT) [47] on the Fermi Gamma-ray Space Telescope, launched in 2008. The LAT is a pair production detector, with a calorimeter that detects a pair production event induced by a gamma ray, determining the arrival direction and energy. It is sensisitive to gamma rays in the range of 20 MeV–300 GeV.

Cosmic ray detection

Searches for other types of highly energetic particles, categorised under the general term of *cosmic rays*, has advantages and disadvantages as compared to that of gamma rays. An advantage in some cases is the weakness of the background signal, as examplified by antimatter particles which are not produced very much by other astrophysical processes. On the other hand, a drawback can be the difficulty in determining the direction of origin of these particles, due to galactic diffusion.

Several current and future projects seek to detect antimatter cosmic rays. PAMELA [48] is a such detector, mounted on a russian satellite, launched in 2006. Another is The Alpha Magnetic Spectrometer (AMS) [49], installed on the International Space Station. Both of these detectors measure the charge (and sign) of a cosmic ray particle.

Neutrino detection

Another type of particle that deserves its own caption is the neutrino. Although they are very difficult to measure and require very large detectors, this very quality is also what makes them useful. Because they pass through matter practically unhindered, they preserve their original energy and direction of motion.

Most neutrino detectors are Cheronkov light detectors. When a neutrino interacts, it can produce a highly energetic muon or electron, much like in the case of gamma rays. While most of the Cherenkov light events come from atmopheric gamma rays, the direction of origin of the signal can be used to exclude this atmospheric background. If the signal is coming from below, it implies that something has travelled through the whole Earth and an atmospheric event can be excluded. A neutrino, however, can travel through the Earth unhindered, and by chance interact in close viscinity to the Cherenkov detector. However, there is a small chance that this neutrino was in fact produced in the atmosphere at the other side of the Earth by some highly energetic cosmic ray. Such a background needs to be excluded.

An example of such a detector is the IceCube neutrino observatory [50], which is a cubic kilometer of photomultiplier buried in the ice cap of the South Pole. With an infill within IceCube called DeepCore [51], its energy therhold is about ~ 10 GeV. A planned upgrade called PINGU will further reduce it to a few GeV. Other famous Cherenkov detectors are ANTARES [52] in the Mediterranean Sea, and Super-Kamiokande [53] in Japan.

Signal sources

An indirect dark matter signal could come from anywhere that the dark matter concentration is significantly dense. Examples are the galactic core, Milky Way satellite dwarf galaxies, or even external galaxies like Andromeda. A signal from black holes could also be relevant, as well as a cosmological signal such as a small peak detracting from the black body spectrum of the CMB.

The source of primary interest for this thesis, however, is that of our own Sun. WIMP annihilation in the Sun would produce a number of highly energetic particles, most of which would not escape the Sun. Neutrinos, however, would escape. Possibly, this flux of high-energy neutrinos from the Sun can be detected. The theory of this phenomena is explored in detail in the next chapter.

3

WIMP Capture by the Sun

In this chapter, I present the theory that has been used and developed during the course of this project: the analytical derivations of WIMP capture by a massive body, an overview of effective field theory and its application in this project, the interaction coefficients limits as given by observational data, and the differential equations that govern the capture and annihilation process.

From here on, it is assumed that the main constituent of the dark matter halo is WIMPs. They are particles that can interact with atomic nuclei via a weak force. WIMPs of the galactic halo would collide with atomic nuclei in the Sun. A fraction of those WIMPs would lose enough kinetic energy to be trapped in orbit. With further collisions with atomic nuclei, they would eventually thermalize and settle in the Sun's core. At some point in time, the concentration of WIMPs within the Sun would be high enough for the them to begin annihilating with each other. This process of decay would produce a flux of high-energy neutrinos.

While the neutrinos produced in the Sun's nuclear fusion process have energy in the MeV range, the neutrinos from annihilated WIMPs would be distinctly different, as their energy would be some fraction of the WIMP mass, in the GeV range. This flux of high-energy neutrinos could then be detected in a neutrino telescope like IceCube. So far no signal has been seen, but larger neutrino telescopes could in a near future be capable of detecting such a signal.

The specific focus of this theses is how the rate of WIMP capture by the Sun and its resulting neutrino flux are affected by also incorporating WIMP self-interaction in the description. A concentration of WIMPs trapped in the Sun's core could itself constitute a scattering target for WIMPs of the galactic halo, given that the self-interaction is strong enough. The goal of this thesis is to find out how large of an amplification to the neutrino flux is possible in the non-excluded parameter space of WIMP-nuclei interaction and WIMP self-interaction. The subject of how self-interaction affects the capture rate is not very well explored in the literature. There is one paper by Zentner [1] which discusses the effects of WIMP self-interaction under the assumption of constant cross-sections.

3.1 WIMP capture rate of a massive body

I begin this discussion by presenting the analytical grounds for dark matter capture. These derivations follow very closely to a of paper by Gould [54], although I abandon the analytical reasoning and proceed with numerical methods at an earlier stage than he does. At first, I have a look at the simplest possible case, which is a massive body at rest, with a constant cross-section. I then generalize these results for a body that is moving with respect to the dark matter halo and for cross-sections that vary with collisional velocity and transferred momentum.

3.1.1 Massive body at rest, constant cross-section

In this section I calculate the total capture rate of a massive body like the Sun, while using some simplifying assumptions. To begin with, I consider a massive body at rest with respect to the dark matter halo. I also assume the cross-section to be constant (independent of relative velocity and transferred momentum).

In order to calculate the total amount of WIMPs passing the massive body, consider the in-flux through an imagined sphere of large radius R, so that the gravity of the massive body is negligible. Let the WIMPs have a velocity distribution $f(u)$, where u is the velocity far away from the massive body. The in-flux through this imagined sphere is then the flux per unit angular area, times angular area, times an angle of inclination factor, which gives

$$\frac{f(u)\,u\,\mathrm{d}u}{4\pi}\cdot 2\pi\sin\theta\,\mathrm{d}\theta\cdot\cos\theta = \frac{1}{4}f(u)\,u\,\mathrm{d}u\,\mathrm{d}\cos^2\theta. \tag{3.1.1}$$

The sign is omitted, as it is a matter of ordering the integration bounds.

The angular momentum per unit mass, $J = Ru\sin\theta$, can be used to rewrite the expression in equation (3.1.1), such that

$$\begin{aligned} \mathrm{d}J^2 &= R^2u^2\,\mathrm{d}\sin^2\theta \\ &= R^2u^2\,\mathrm{d}(1-\cos^2\theta) \\ &= -R^2u^2\,\mathrm{d}\cos^2\theta. \end{aligned} \tag{3.1.2}$$

Again, the sign change can be accounted for by choosing the integration bounds, so that J^2 goes from 0 (lower bound) to R^2u^2 (upper bound). Integrating over the sphere's surface at radius R gives the in-going flux,

$$4\pi R^2 \frac{1}{4} f(u)\, u \,\mathrm{d}u \,\frac{\mathrm{d}J^2}{R^2 u^2} = \pi \frac{f(u)\,\mathrm{d}u}{u} \mathrm{d}J^2. \tag{3.1.3}$$

Consider the capture rate of one thin spherical shell of matter, of radius r and thickness $\mathrm{d}r$. Let v be the escape velocity at that shell. The velocity of a WIMP that reaches that shell is $w = \sqrt{u^2+v^2}$. To reach the shell at all, there is a condition that $J < rw$. The shell surface is hit with an inclination angle θ', meaning that the WIMP travels a distance within the shell of

$$2\mathrm{d}r(\cos\theta')^{-1} = \{J = rw\sin\theta'\} = 2\mathrm{d}r\left[1 - (\frac{J}{rw})^2\right]^{-1/2}. \tag{3.1.4}$$

The factor 2 comes from the particle going through the shell twice, as the particle also goes out.

To be captured, a WIMP has to scatter to less than escape velocity, v. Define $\Omega_v^-(w)$ to be the probability per unit time that this scattering occurs, which divided by velocity becomes the probability per unit length. The probability of a WIMP being trapped by scattering in the thin shell of radius r is then

$$\frac{\Omega_v^-(w)}{w} 2\mathrm{d}r\left[1 - (\frac{J}{rw})^2\right]^{-1/2} \theta(rw - J). \tag{3.1.5}$$

Multiplying this quantity by the total in-flux from equation (3.1.3) and integrating over all angular momenta gives

$$\begin{aligned}
&\int_{J^2=0}^{J^2=(rw)^2} \pi\frac{f(u)\,\mathrm{d}u}{u}\mathrm{d}J^2 \frac{\Omega_v^-(w)}{w} 2\mathrm{d}r\left[1-(\frac{J}{rw})^2\right]^{-1/2} = \\
&= 2\pi\frac{f(u)\,\mathrm{d}u}{u}\frac{\Omega_v^-(w)}{w}\mathrm{d}r\int_{J^2=0}^{J^2=(rw)^2}\left[1-(\frac{J}{rw})^2\right]^{-1/2}\mathrm{d}J^2 = \\
&= \{\text{Substitute: } \frac{J^2}{r^2w^2} = s\} = \\
&= 2\pi\frac{f(u)\,\mathrm{d}u}{u}\frac{\Omega_v^-(w)}{w}\mathrm{d}r\int_{s=0}^{s=1} r^2w^2\frac{\mathrm{d}s}{\sqrt{1-s}} = \\
&= 2\pi\frac{f(u)\,\mathrm{d}u}{u}\frac{\Omega_v^-(w)}{w}\mathrm{d}r\, r^2w^2[-2\sqrt{1-s}]_0^1 = \\
&= 4\pi r^2\mathrm{d}r\frac{f(u)\,\mathrm{d}u}{u}w\Omega_v^-(w).
\end{aligned} \tag{3.1.6}$$

This is the number of WIMPs captured by the shell per unit time per unit velocity. The factor $4\pi r^2\mathrm{d}r$ is precisely the volume of the shell. Thus, the total capture rate per unit volume is

$$\frac{\mathrm{d}C}{\mathrm{d}V} = \int_0^\infty \frac{f(u)}{u} w \Omega_v^-(w) \mathrm{d}u. \tag{3.1.7}$$

Here it is implicit that w (WIMP velocity at the shell) is a function of u (WIMP velocity at infinite radius) and v (escape velocity at the shell), where v varies with radius.

Given the velocity distribution $f(u)$ and the escape velocity at the shell's radius, all that remains is to write out the quantity $\Omega_v^-(w)$, the probability per unit time to scatter to less than escape velocity. In the simplest case of constant cross-section, we have a total scattering probability of $\sigma n w$, where σ is the cross-section and n is the target number density in the shell. What is sought, however, is not the total cross-section, but the cross-section times the probability that a scattering event results in a velocity lower than escape velocity.

In the case of a constant cross-section, this is fairly straight forward. Consider a inertial frame where the target nucleus is at rest. The maximum kinetic energy transferred to the nucleus occurs in a head-on collision. The kinematics of an elastic collision in one dimension gives that

$$\left.\frac{\Delta E}{E}\right|_{\max} = \frac{4 M_\chi m_N}{(M_\chi + m_N)^2}, \tag{3.1.8}$$

where m_N is the mass of the target nucleus and M_χ is the mass of the incoming WIMP. On the other hand, if the WIMP is barely grazing the target nucleus then the transferred kinetic energy can be arbitrarily small, so that the minimum transferred energy in a collision is zero. Furthermore, the probability density for the collision is evenly distributed with respect to ΔE, which can be realized by looking at the phase-space of the target nucleus after the collision, for which all collisional angles are equally probable.

Because the loss of energy must be such that the particle scatters to below escape velocity, there is a requirement that

$$\frac{\Delta E}{E} \geq \frac{w^2 - v^2}{w^2} = \frac{u^2}{w^2}. \tag{3.1.9}$$

Thus the probability that a scattering event lead to capture is simply

$$P_{\text{capt.}} = 1 - \left(\frac{4 M_\chi m_N}{(M_\chi + m_N)^2} \right)^{-1} \frac{u^2}{w^2}. \tag{3.1.10}$$

There is a condition for this quantity to be positive, as otherwise capture is not kinematically possible.

The rate of scattering that results in capture is thus the total rate of scattering, $\sigma n w$, times the above probability and condition, which gives

$$\Omega_v^- = \sigma n w \left(1 - \frac{(M_\chi + m_N)^2}{4M_\chi m_N}\frac{u^2}{w^2}\right)\theta\left(1 - \frac{(M_\chi + m_N)^2}{4M_\chi m_N}\frac{u^2}{w^2}\right), \tag{3.1.11}$$

where $\theta(...)$ is the Heaviside step function.

To simplify the integral in equation (3.1.7), I rewrite this expression so that the integrand has no w dependence, like

$$\Omega_v^- = \frac{\sigma n}{w}\left(v^2 - \frac{(M_\chi - m_N)^2}{4M_\chi m_N}u^2\right)\theta\left(v^2 - \frac{(M_\chi - m_N)^2}{4M_\chi m_N}u^2\right). \tag{3.1.12}$$

Now the factor w^{-1} cancels against the factor w in the integral of equation (3.1.7).

For the sake of simplicity I assume the WIMP velocity distribution to be Maxwellian and that the massive body is stationary with respect to the WIMP halo rest frame. The velocity distribution is

$$f(u)\mathrm{d}u = n_\chi \frac{4}{\sqrt{\pi}} x^2 e^{-x^2}\mathrm{d}x, \tag{3.1.13}$$

where n_χ is the WIMP number density and $x^2 = 3(u/\bar{v})^2/2$ is the dimensionless velocity, where $\bar{v}$ is the velocity dispersion.

To further simplify the integrand expression in equation (3.1.12), I define a quantity

$$A^2 = \frac{3}{2}\frac{v^2}{\bar{v}^2}\frac{4M_\chi m_N}{(M_\chi - m_N)^2}, \tag{3.1.14}$$

which through the Heaviside-function in Ω_v^- constitutes the upper limit of the integral. The integral is now

$$
\begin{aligned}
\frac{\mathrm{d}C}{\mathrm{d}V} &= \int_0^{x=A} n_\chi \frac{4}{\sqrt{\pi}} x^2 e^{-x^2} \frac{\sigma n}{u} \left(v^2 - \frac{(M_\chi - m_N)^2}{4M_\chi m_N} u^2 \right) \mathrm{d}x = \\
&= \int_0^{A} n_\chi \frac{4}{\sqrt{\pi}} x^2 e^{-x^2} \sqrt{\frac{3}{2}} \frac{\sigma n}{\bar{v} x} \left(v^2 - \frac{(M_\chi - m_N)^2}{4M_\chi m_N} \frac{2}{3} \bar{v}^2 x^2 \right) \mathrm{d}x = \\
&= \int_0^{A} n_\chi \sqrt{\frac{24}{\pi}} e^{-x^2} \frac{\sigma n}{\bar{v}} \left(v^2 x - \frac{(M_\chi - m_N)^2}{4M_\chi m_N} \frac{2}{3} \bar{v}^2 x^3 \right) \mathrm{d}x = \\
&= \int_0^{A} n_\chi \sqrt{\frac{24}{\pi}} e^{-x^2} \frac{\sigma n}{\bar{v}} v^2 \left(x - A^{-2} x^3 \right) \mathrm{d}x = \\
&= \left\{ \begin{aligned} &\int_0^A x e^{-x^2} \mathrm{d}x = \frac{1}{2}(1 - e^{-A^2}) \\ &\int_0^A x^3 e^{-x^2} \mathrm{d}x = \frac{1}{2}\Big(1 - (A^2+1)e^{-A^2}\Big) \end{aligned} \right\} = \\
&= n_\chi \sqrt{\frac{6}{\pi}} \frac{\sigma n}{\bar{v}} v^2 \left(1 - \frac{1 - e^{-A^2}}{A^2} \right).
\end{aligned}
\tag{3.1.15}
$$

Finding the total capture rate is now a matter of integrating over the total volume of the Sun, like

$$
\begin{aligned}
C &= \int_0^{R_\odot} 4\pi r^2 \frac{\mathrm{d}C}{\mathrm{d}V} \mathrm{d}r \\
&= 4\pi n_\chi \sqrt{\frac{6}{\pi}} \frac{\sigma}{\bar{v}} \int_0^{R_\odot} r^2 n v^2 \left(1 - \frac{1 - e^{-A^2}}{A^2} \right) \mathrm{d}r.
\end{aligned}
\tag{3.1.16}
$$

The nucleon density n, the escape velocity v and the dimensionless quantity A (directly proportional to v) in the integrand are the only quantities that depend on the radius. With these quantities at hand, the integral can be evaluated numerically. The different isotopes in the Sun would be integrated over separately, as they have different densities, particle masses, and cross-sections.

3.1.2 Massive body in motion

An added complication to the result presented above is if the massive body is moving with respect to the WIMP halo. If we stay in the rest frame of the massive body, then the velocity distribution of the WIMP halo must be translated by their relative velocities. To translate the Maxwellian distribution, I can rewrite it as an integral over spherical angles, like

$$
\begin{aligned}
f(u)\mathrm{d}u &= n_\chi \frac{4}{\sqrt{\pi}} x^2 e^{-x^2} \mathrm{d}x = \\
&= n_\chi \frac{4}{\sqrt{\pi}} \int e^{-x^2} x^2 \mathrm{d}x \frac{\mathrm{d}(\cos\theta)\mathrm{d}\phi}{4\pi}.
\end{aligned} \tag{3.1.17}
$$

The part $x^2\mathrm{d}x$ is the Jacobian in spherical coordinates and should not be affected by the change of inertial frame. Rather, it is only the term e^{-x^2} that is changed, for which $x^2 \to x_x^2 + x_y^2 + (x_z + \eta)^2 = x^2 + 2\eta x \cos\theta + \eta^2$. The quantity η has the same normalization as x, such that $\eta^2 = 3(v_\odot/\bar{v})^2/2$, where $v_\odot$ is the velocity of the massive body as seen from the rest frame of the WIMP halo. The result is

$$
\begin{aligned}
f(u)\mathrm{d}u \to n_\chi \frac{4}{\sqrt{\pi}} &\int e^{-x^2} e^{-\eta^2} e^{-2\eta x \cos\theta} x^2 \mathrm{d}x \frac{\mathrm{d}(\cos\theta)\mathrm{d}\phi}{4\pi} = \\
&= n_\chi \frac{4}{\sqrt{\pi}} e^{-x^2} e^{-\eta^2} x^2 \mathrm{d}x \frac{1}{2} \left[-\frac{1}{2x\eta} e^{-2x\eta\cos\theta} \right]_{\cos\theta=-1}^{\cos\theta=1} = \\
&= n_\chi \frac{4}{\sqrt{\pi}} e^{-x^2} e^{-\eta^2} x^2 \mathrm{d}x \frac{e^{2x\eta} - e^{-2x\eta}}{4x\eta} = \\
&= n_\chi \frac{4}{\sqrt{\pi}} e^{-x^2} x^2 \mathrm{d}x \, e^{-\eta^2} \frac{\sinh 2x\eta}{2x\eta}.
\end{aligned} \tag{3.1.18}
$$

This is the new velocity distribution that must be used. It makes the integral of equation (3.1.7), the capture rate per unit volume, more lengthy to calculate analytically. I do not present these results here, however, as in this project these integrals are evaluated numerically anyway.

3.1.3 Capture rates with varying cross-section

In this section I will generalize the expression of the Sun's total capture rate, from the case of a constant cross-section to a cross-section that varies with collisional velocity and transferred momentum. In the case of a constant cross-section, the total rate of scattering is $\sigma n w$. Multiplying this quantity by the fraction of transferred kinetic energy that results in capture gives the total probability of capture per unit time, Ω_v^-, as seen in equation (3.1.11).

In the generalized case, the cross-section varies with collisional velocity and transferred kinetic energy (or equally well with transferred momentum or angle of scattering). This necessitates a description by means of differential cross-section, $\mathrm{d}\sigma/\mathrm{d}E_r$, which can be integrated over to retain the total cross-section or the total rate of scattering that results in capture.

With these considerations, in analogy with equation (3.1.11), the rate of scattering from a velocity w to a velocity less than escape velocity v per unit time becomes

$$\Omega_v^-(w) = nw\,\theta\left(1 - \frac{(M_\chi + m_N)^2}{4M_\chi m_N}\frac{u^2}{w^2}\right)\int_{M_\chi u^2/2}^{\frac{2M_\chi^2 m_N w^2}{(M_\chi+m_N)^2}} \mathrm{d}E_r \frac{\mathrm{d}\sigma}{\mathrm{d}E_r}(w,E_r). \tag{3.1.19}$$

The lower limit of the integral is the minimal energy that the WIMP must lose in order to be captured; the upper limit is the highest energy transfer that is kinematically possible in an elastic collision.

In analogy with the case of the constant cross-section, the capture rate per unit volume is

$$\frac{\mathrm{d}C}{\mathrm{d}V} = \int_0^\infty \mathrm{d}u \frac{f(u)}{u} w\Omega_v^-(w), \tag{3.1.20}$$

where the upper limit of the integral in effect is given by the Heaviside-function in Ω_v^-. The total capture rate is, just like before,

$$C = \int_0^{R_\odot} 4\pi r^2 \frac{\mathrm{d}C}{\mathrm{d}V}\mathrm{d}r. \tag{3.1.21}$$

These integrals are performed numerically for each isotope species of target nuclei. The differential cross-sections are calculated by means of effective field theory. Further information on effective field theory and differential cross-sections is found in section 3.2.

3.1.4 Solar densities and cold static body approximation

When calculating the capture rates in this thesis, I account for the 16 most abundant elements of the Sun, as seen in table 3.1 with their respective mass fractions. The solar densities for the different isotopes, with radial dependence, are taken from the standard solar model [55], also used in the DarkSUSY package [56]. I approximate the Sun as being static, meaning that I do not account for the fact that these densities have changed over time. The total helium mass fraction has changed only slightly during its lifetime, from ~ 27 % to ~ 30 %. The relative change in metallicity is even smaller. This justifies the approximation of the Sun as static, using current isotope densities.

In the evaluation of the capture rate, I also approximate the massive body as being cold. The target particle is assumed to be stationary, so that its thermal movement within the massive body is neglected. Thus the collisional velocity is solely determined by the velocity of the in-falling WIMP. Comparing the general

Isotope	Mass fraction	Isotope	Mass fraction
H	0.684	^{24}Mg	$7.30 \cdot 10^{-4}$
^{4}He	0.298	^{27}Al	$6.38 \cdot 10^{-5}$
^{3}He	$3.75 \cdot 10^{-4}$	^{28}Si	$7.95 \cdot 10^{-4}$
^{12}C	$2.53 \cdot 10^{-3}$	^{32}S	$5.48 \cdot 10^{-4}$
^{14}N	$1.56 \cdot 10^{-3}$	^{40}Ar	$8.04 \cdot 10^{-5}$
^{16}O	$8.50 \cdot 10^{-3}$	^{40}Ca	$7.33 \cdot 10^{-5}$
^{20}Ne	$1.92 \cdot 10^{-3}$	^{56}Fe	$1.42 \cdot 10^{-3}$
^{23}Na	$3.94 \cdot 10^{-5}$	^{59}Ni	$8.40 \cdot 10^{-5}$

Table 3.1: The 16 most abundant isotopes of the Sun and their total mass fractions.

magnitude of these velocities shows that the thermal movement is completely negligable in most cases and a fair approximation in others. The escape velocity of the Sun is about 620 km/s at the surface and 1380 km/s at the core, which constitutes the minimum impact velocity of an in-falling WIMP at that radius. The core temperature of the Sun is $1.57 \cdot 10^7$ K, meaning that the lightest nuclei would have a velocity dispersion of a few hundred km/s in the core, which can be considered a relatively small correction factor to the overall picture. In the most extreme case, which is for hydrogen, the correction is at most a few percent. This accuracy is still more exact than for many other parameters, such as the WIMP halo density, which is why I proceed under a cold body approximation.

3.1.5 Self-capture rate

The self-capture rate is calculated much like in the previous section 3.1.3. However, there are minor differences to be accounted for.

It is assumed that a WIMP that scatters to less than escape velocity will soon scatter again and quickly thermalize, settling in the core of the Sun. The use of the term "quickly" is meant in relation to the billion year time-scale of building up a concentration of trapped WIMPs within the Sun. A rough order-of-magnitude estimate is enough to justify this assumption. A WIMP that loses only 10 % of its total kinetic energy in a collision in the Sun's core will be bound in orbit such that it travels through the Sun more than two thousand times per year. There is a one-in-a-billion probability to scatter off of hydrogen when going through the Sun's core, assuming a cross-section of 10^{-45} cm^2. This gives an average of half a million years before its second scattering event, after which the process will be even quicker. Therefore, it is safe to say that only very improbable and rare events will take billions of years to thermalize.

It is assumed that the trapped WIMPs thermilize to the Sun's core temperature. Even with strong WIMP self-interaction, the rate of in-flowing kinetic energy by WIMPs would be lower than the rate of energy they lose in the thermalization process. Therefore, I use a thermal profile for the captured WIMPs,

$$\epsilon(r) \propto \exp\left[-\frac{M_\chi \phi(r)}{T_{\mathrm{core}}}\right], \tag{3.1.22}$$

where ϵ is the WIMP density as a function of radius, given by the WIMP mass, the gravitational potential, and the Sun's core temperature. Even for a very light dark matter particle of mass 10 GeV, captured and thermalized WIMPs are confined to about one percent of the Sun's radius.

If self-interaction is present and significant there could potentially be a degree of evaporation. There is a possibility that an in-falling WIMP could collide with a target WIMP and distribute the kinetic energy such that they both escape the gravitational well of the massive body. It turns out for the case of the Sun that this is a very insignificant factor, many orders of magnitude smaller than the total capture by self-interaction. This is due to the Sun's large escape velocity. However, for a less massive body, such as the Earth, this effect could be very important.

What is more significant than evaporation is the case where the in-falling WIMP is captured but the target WIMP escapes. This would happen, for example, in a head-on collision where the two WIMPs simply exchange kinetic energy. Such an event results in a status quo: no net gain or loss of captured WIMPs. This effect is accounted for by setting an upper limit in the integral, $M_\chi v^2/2$, which is the energy needed in order to escape.

Because the in-falling particle and the target particle are identical and have the same mass, the expression becomes somewhat tidier compared to WIMP capture by nuclei. The integral, analogous to equation (3.1.19), becomes

$$\Omega_v^-(w) = \epsilon(r) w\, \theta(v^2 - u^2) \int_{M_\chi u^2/2}^{M_\chi v^2/2} \mathrm{d}E_r \frac{\mathrm{d}\sigma_{\chi\chi}}{\mathrm{d}E_r}(w, E_r), \tag{3.1.23}$$

where $\epsilon(r)$ is the WIMP number density of equation (3.1.22) and $\sigma_{\chi\chi}$ is the WIMP self-interaction cross-section.

3.1.6 Annihilation rate

Annihilation of captured WIMPs within the Sun will come into effect when the concentration has become sufficiently high. The annihilation cross-section of a non-relativistic relic dark matter particle comes from cosmological arguments. This

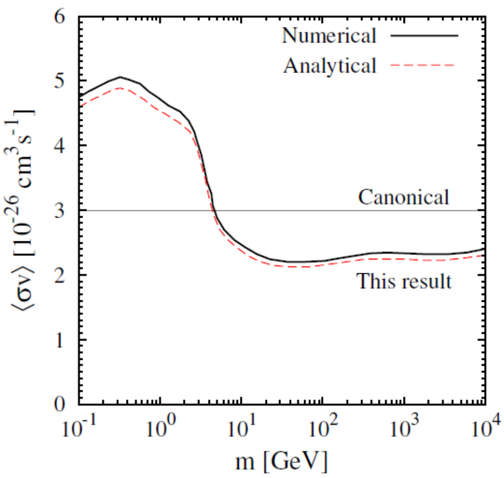

Figure 3.1: The thermal annihilation cross-section as a function of WIMP mass. The result is fairly constant in the mass range of 10–1000 GeV, and somewhat lower than the canonical value. The analytical and numerical evaluations differ by less than 3 %. The figure is from an article by Steigman, Dasgupta, and Beacom [27].

quantity multiplied by the number density squared, ϵ^2, becomes the annihilation rate per unit volume.

A canonical value for the thermally averaged annihilation cross-section is $\langle \sigma_A v \rangle \simeq 3 \cdot 10^{-26}$ cm^{3}s^{-1}. However, recent studies have made more precise evaluations of this value [27], as can be seen in figure 3.1. Following these results, the value used in this thesis is $\langle \sigma_A v \rangle \simeq 2 \cdot 10^{-26}$ cm^{3}s^{-1}.

Thus the total annihilation rate of the Sun is proportional to an annihilation factor, C_a, and the total number of captured WIMPs squared, N^2. The annihilation factor is

$$C_a = \frac{4\pi \langle \sigma_A v \rangle}{N^2} \int_0^{R_\odot} \epsilon^2(r) r^2 \mathrm{d}r, \tag{3.1.24}$$

with unit s^{-1}.

Because the WIMP distribution is so localized in the solar interior and the core of the Sun has more or less a constant density, the annihilation factor follows closely the analytical form

$$C_a = 2.8 \cdot 10^{-57} \left(\frac{M_\chi}{\mathrm{GeV}} \right)^{3/2} \mathrm{s}^{-1}. \tag{3.1.25}$$

The total amount of annihilation events in the Sun is $C_a N^2/2$, where the factor 1/2 is due to that WIMPs annihilate in pairs. The differential neutrino flux produced by these annihilation events is [22]

$$\frac{\mathrm{d}\Phi_\nu}{\mathrm{d}E_\nu} = \frac{1}{4\pi D^2}\frac{C_a N^2}{2}\sum_f B_\chi^f \frac{\mathrm{d}N_\nu^f}{\mathrm{d}E_\nu}, \tag{3.1.26}$$

where E_ν is the neutrino energy, D is the distance from the Sun, B_χ^f is the branching ratio for WIMP pair annihilation, and $\mathrm{d}N_\nu^f/\mathrm{d}E_\nu$ is the neutrino energy spectrum produced by decay channel f.

Neutrinos coming from WIMP annihilation in the Sun can be detected in a neutrino telescope on Earth. Such a detector measures an upward muon flux induced by neutrinos interacting with nuclei in the surrounding material. The differential muon flux is [57]

$$\frac{\mathrm{d}\Phi_\mu}{\mathrm{d}E_\mu} = N_T \int_{E_\mu^{\mathrm{th}}}^{\infty} \mathrm{d}E_\nu \int_0^\infty \mathrm{d}\lambda \int_{E_\mu}^{E_\mu} \mathrm{d}E'_\mu \; \mathcal{P}(E_\mu, E'_\mu; \lambda) \; \frac{\mathrm{d}\sigma_{CC}(E_\nu, E'_\mu)}{\mathrm{d}E'_\mu} \frac{\mathrm{d}\Phi_\nu}{\mathrm{d}E_\nu}, \tag{3.1.27}$$

where N_T is the nucleon number density in the material surrounding the detector, E_μ^{th} is the detector energy threshold, λ is the muon range, $\mathcal{P}(E_\mu, E'_\mu; \lambda)$ is the probability of a muon of initial energy E'_μ to have final energy E_μ after traveling a distance λ inside the detector, and $\mathrm{d}\sigma_{CC}(E_\nu, E'_\mu)/\mathrm{d}E'_\mu$ is the weak differential cross-section for production of a muon with energy E'_μ.

These expressions are not a prime concern of this thesis, as only a *relative amplification* to the neutrino signal is sought.

3.2 Effective field theory

An effective field theory (EFT) is an approximate description of a physical system or field theory, viable in restricted volume of its parameter space, typically in a low-energy limit. An EFT description is made possible in a system of widely separated scales, for example when high energy effects can be regarded as perturbations with respect to the dominating low energy behavior. This is an indispensable tool and standard procedure for a lot of applications in field theory. It is widely believed that the Standard Model itself is an effective theory, in that it operates in a low-energy limit of some higher and unknown, possibly unified, physics.

The EFT approach can be used both when the full theory is known and when it is unknown. In the case that the full theory is known, it is possible to integrate out the heavy modes and treat their influence perturbatively. Consider a simple example of a field theory of one very heavy field, Φ, and one very light field, ϕ, described by a functional $S[\phi,\Phi]$. The heavy field can be integrated out,

$$e^{iS_{eff}[\phi]} = \int e^{iS[\phi,\Phi]} D\Phi, \tag{3.2.1}$$

to produce a local effective functional for the low energy field. This effective functional can be expressed as a series of interaction operators,

$$S_{eff}[\phi] = \sum_i c_i \int \mathrm{d}x^4 \mathcal{O}_i(x). \tag{3.2.2}$$

The coefficients c_i are infinitely many, but they scale as increasing factors of the ratio between energy scales. This is what allows for a perturbative treatment. An example of such a procedure would be to reduce the full electroweak field theory to a electromagnetic EFT with weak-force interaction operators. This is possible due to the operating energy scale of the system being much lower than the mass of the weak-force W and Z bosons.

Even if the physics of the full theory and its behavior at high energy is unknown, EFT can be applied. By writing down all operators that respect the symmetries of the physical system at low energy, it is possible to construct a completely general and model-independent description of the theory. This is also the approach that is used in this thesis, as the theory of WIMP interactions is not known (although there are various models). For WIMPs captured by the Sun, the relevant interactions are the in non-relativistic regime. Hence, an EFT in the limit of Newtonian physics, with operators respecting Galilean symmetry, allows for a model-independent exploration of parameter space.

3.2.1 Non-relativistic interaction operators

The possible quantum operators that dictate the interaction between particles are restricted by physical symmetries. Elastic collisions in the non-relativistic limit must conserve energy and momentum, and adhere to the symmetries of Galilean invariance (a Galilean transformation is a shift of all particles by some three dimensional spatial velocity). This restriction leads to a finite number of possible leading order interaction operators.

Any such interaction term is constructed from these five Hermitian quantum operators,

$$\mathbb{1}_{\chi N} \qquad i\hat{\mathbf{q}} \qquad \hat{\mathbf{v}}^{\perp} \qquad \hat{\mathbf{S}}_{\chi} \qquad \hat{\mathbf{S}}_{N}. \tag{3.2.3}$$

For the sake of clarity, the two particles involved in the collision are assumed to be a WIMP and a nucleon, denoted with indices χ and N, although they could really be of any type. Later on, self-interaction between two WIMPs is also considered.

These five operators are invariant with respect to Galilean transformation. The first, fourth and fifth are trivially invariant, as a Galilean transformation leaves the spin unaffected. The second operator is the transferred momentum of the collision, $\mathbf{q} \equiv \mathbf{k} - \mathbf{k}'$, where $\mathbf{k}$ is the momentum of a particle before collision and $\mathbf{k}'$ is that same particle's momentum after collision. Quantum mechanically the operator yields

$$\langle \mathbf{p}', j_\chi; \mathbf{k}', j_N | i\hat{\mathbf{q}} | \mathbf{p}, j_\chi; \mathbf{k}, j_N \rangle = i\mathbf{q} e^{-i\mathbf{q}\cdot\mathbf{r}} (2\pi)^3 \delta(\mathbf{k}' + \mathbf{p}' - \mathbf{k} - \mathbf{p}). \tag{3.2.4}$$

The third operator is the transverse velocity and perhaps less obviously a Galilean invariant quantity. More intuitively realized is that the relative velocity before collision, $\mathbf{v} \equiv \mathbf{p}/m_\chi - \mathbf{k}/m_N$, is invariant. The transverse velocity is formed to be invariant, $\mathbf{v}^\perp \equiv \mathbf{v} + \mathbf{q}/(2\mu)$, where μ is the reduced mass of the two-particle system. The quantum operator yields

$$\langle \mathbf{p}', j_\chi; \mathbf{k}', j_N | \hat{\mathbf{v}}^\perp | \mathbf{p}, j_\chi; \mathbf{k}, j_N \rangle = \left(\mathbf{v} + \frac{\mathbf{q}}{2\mu} \right) \mathbf{q} e^{-i\mathbf{q}\cdot\mathbf{r}} (2\pi)^3 \delta(\mathbf{k}' + \mathbf{p}' - \mathbf{k} - \mathbf{p}). \tag{3.2.5}$$

These five quantum operators can be combined in different ways to form Galilean invariant interaction operators. There is a demand for them to be of leading order, and to be at most linear in $\hat{\mathbf{S}}_\chi$, $\hat{\mathbf{S}}_N$, and $\hat{\mathbf{v}}^\perp$. The restriction on the spin and transverse momentum comes from the mediating particle of the full theory, which is assumed to have spin 1 or lower. The complete list of such operators is visible in table 3.2, where the mass m_N has been utilized to make the operators dimensionless. The indices follow the convention of Haxton *et al.* [58] and Catena and Schwabe [59], such that the operator $\hat{\mathcal{O}}_2 = \hat{\mathbf{v}}^\perp \cdot \hat{\mathbf{v}}^\perp$ is excluded from the list. The 14 operators all correspond to a linear combination of operators in the relativistic theory. For example, the operator $\hat{\mathcal{O}}_{10}$ is obtained from the interaction term $i\bar{\chi}\chi\bar{N}\gamma^5 N$ in its non-relativistic limit.

The total Hamiltonian density in the effective field theory is thus

$$\hat{\mathcal{H}}(\mathbf{r}) = \sum_{k=1}^{15} c_k \hat{\mathcal{O}}_k(\mathbf{r}). \tag{3.2.6}$$

The coefficients c_k are coupling constants and have dimension mass^{-2}. The end goal of this chapter is to obtain the differential cross-section, $\mathrm{d}\sigma/\mathrm{d}E_R$, as a function of this linear combination of operators. This is done by squaring the scattering amplitude, $\mathcal{M}$, and integrating over all free variables. This is complicated enough in its own right, but made even more so for the case of atomic nuclei made up of several nucleons. The inner structure of the nucleus and the resulting scattering resonances must be accounted for. By describing this inner structure by means of form factors, a nucleus can still be treated as a single particle.

$\hat{\mathcal{O}}_1 = \mathbb{1}_{\chi N}$	$\hat{\mathcal{O}}_9 = i\hat{\mathbf{S}}_\chi \cdot \left(\hat{\mathbf{S}}_N \times \frac{\hat{\mathbf{q}}}{m_N}\right)$
$\hat{\mathcal{O}}_3 = i\hat{\mathbf{S}}_N \cdot \left(\frac{\hat{\mathbf{q}}}{m_N} \times \hat{\mathbf{v}}^\perp\right)$	$\hat{\mathcal{O}}_{10} = i\hat{\mathbf{S}}_N \cdot \frac{\hat{\mathbf{q}}}{m_N}$
$\hat{\mathcal{O}}_4 = \hat{\mathbf{S}}_\chi \cdot \hat{\mathbf{S}}_N$	$\hat{\mathcal{O}}_{11} = i\hat{\mathbf{S}}_\chi \cdot \frac{\hat{\mathbf{q}}}{m_N}$
$\hat{\mathcal{O}}_5 = i\hat{\mathbf{S}}_\chi \cdot \left(\frac{\hat{\mathbf{q}}}{m_N} \times \hat{\mathbf{v}}^\perp\right)$	$\hat{\mathcal{O}}_{12} = \hat{\mathbf{S}}_\chi \cdot \left(\hat{\mathbf{S}}_N \times \hat{\mathbf{v}}^\perp\right)$
$\hat{\mathcal{O}}_6 = \left(\hat{\mathbf{S}}_\chi \cdot \frac{\hat{\mathbf{q}}}{m_N}\right)\left(\hat{\mathbf{S}}_N \cdot \frac{\hat{\mathbf{q}}}{m_N}\right)$	$\hat{\mathcal{O}}_{13} = i\left(\hat{\mathbf{S}}_\chi \cdot \hat{\mathbf{v}}^\perp\right)\left(\hat{\mathbf{S}}_N \cdot \frac{\hat{\mathbf{q}}}{m_N}\right)$
$\hat{\mathcal{O}}_7 = \hat{\mathbf{S}}_N \cdot \hat{\mathbf{v}}^\perp$	$\hat{\mathcal{O}}_{14} = i\left(\hat{\mathbf{S}}_\chi \cdot \frac{\hat{\mathbf{q}}}{m_N}\right)\left(\hat{\mathbf{S}}_N \cdot \hat{\mathbf{v}}^\perp\right)$
$\hat{\mathcal{O}}_8 = \hat{\mathbf{S}}_\chi \cdot \hat{\mathbf{v}}^\perp$	$\hat{\mathcal{O}}_{15} = -\left(\hat{\mathbf{S}}_\chi \cdot \frac{\hat{\mathbf{q}}}{m_N}\right)\left[\left(\hat{\mathbf{S}}_N \times \hat{\mathbf{v}}^\perp\right) \cdot \frac{\hat{\mathbf{q}}}{m_N}\right]$

Table 3.2: All leading order non-relativistic interaction operators.

3.2.2 WIMP-nuclei interaction

For interactions between WIMPs and nuclei, the parameter space of possible interaction coefficients is doubled, as there are two types of nucleons: protons and neutrons. The WIMP-nucleon Hamiltonian density can be written in a basis of isospin, represented by an upper index τ, which is 0 for isoscalar and 1 for isovector coupling constant. By labeling each of nucleons with an index i, the total Hamiltonian density for the nucleus of mass number A can be written

$$\hat{\mathcal{H}}(\mathbf{r}) = \sum_{i=1}^{A} \sum_{\tau=0,1} \sum_{k=1}^{15} c_k^\tau \hat{\mathcal{O}}_k^{(i)}(\mathbf{r}) t_{(i)}^\tau. \tag{3.2.7}$$

The quantity $t_{(i)}^\tau$ is a matrix that projects a nucleon state onto a isospin or isoscalar state. If changing to a basis of proton and neutron couplings, the coupling coefficients are related like $c_k^p = (c_k^0 + c_k^1)/2$ and $c_k^n = (c_k^0 - c_k^1)/2$.

To account for the inner structure of a nucleus, it is convenient to separate its position, denoted $\mathbf{x}$, to the relative position of a target nucleon inside it, $\mathbf{r}$. Let $\mathbf{y}$ represent the position of a WIMP. The quantum mechanical operators can be rewritten like

$$\hat{\mathbf{q}} = -i\overleftarrow{\nabla}_{\mathbf{x}}\delta(\mathbf{x} - \mathbf{y} + \mathbf{r}) - i\delta(\mathbf{x} - \mathbf{y} + \mathbf{r})\overrightarrow{\nabla}_{\mathbf{x}} \tag{3.2.8}$$

$$\hat{\mathbf{v}}^\perp = \hat{\mathbf{v}}_T^\perp + \hat{\mathbf{v}}_N^\perp, \tag{3.2.9}$$

where

$$\hat{\mathbf{v}}_T^{\perp} = \delta(\mathbf{x} - \mathbf{y} + \mathbf{r}) \left(i\frac{\overrightarrow{\nabla}_{\mathbf{x}}}{m_T} - i\frac{\overrightarrow{\nabla}_{\mathbf{y}}}{m_\chi} \right) + \frac{1}{2\mu_T}\hat{\mathbf{q}} \tag{3.2.10}$$

$$\hat{\mathbf{v}}_N^{\perp} = \frac{1}{2m_N} \left(i\overleftarrow{\nabla}_{\mathbf{r}}\delta(\mathbf{r} - \mathbf{r}_i) - i\delta(\mathbf{r} - \mathbf{r}_i)\overrightarrow{\nabla}_{\mathbf{r}} \right). \tag{3.2.11}$$

Here, m_T is the target nucleus mass and μ_T is the WIMP-nucleus reduced mass. The operator $\nabla_{\mathbf{r}}$ acts on the constituent target nucleon. This separation is useful as $\mathbf{r}$ is the only operator that depends on the position of the individual nucleon, $\mathbf{r}$. Any interaction operator not containing $\hat{\mathbf{v}}_N^{\perp}$ acts like identity on quantity $\mathbf{r}$, meaning that it is not coupled to the internal structure of the nucleus.

Using this, it is possible to rewrite equation (3.2.7) to the form

$$\begin{aligned}
\hat{\mathcal{H}}(\mathbf{r}) = \sum_{\tau=0,1} \Bigg\{ & \sum_{i=1}^{A} \hat{l}_0^\tau \delta(\mathbf{r} - \mathbf{r_i}) \\
& + \sum_{i=1}^{A} \hat{l}_{0A}^\tau \frac{1}{2m_N} \left(i\overleftarrow{\nabla}_{\mathbf{r}} \cdot \vec{\sigma}(i)\delta(\mathbf{r} - \mathbf{r}_i) - i\delta(\mathbf{r} - \mathbf{r}_i)\vec{\sigma}(i) \cdot \overrightarrow{\nabla}_{\mathbf{r}} \right) \\
& + \sum_{i=1}^{A} \hat{\mathbf{l}}_5^\tau \cdot \vec{\sigma}(i)\delta(\mathbf{r} - \mathbf{r_i}) \\
& + \sum_{i=1}^{A} \hat{\mathbf{l}}_M^\tau \frac{1}{2m_N} \left(i\overleftarrow{\nabla}_{\mathbf{r}}\delta(\mathbf{r} - \mathbf{r}_i) - i\delta(\mathbf{r} - \mathbf{r}_i)\overrightarrow{\nabla}_{\mathbf{r}} \right) \\
& + \sum_{i=1}^{A} \hat{\mathbf{l}}_E^\tau \frac{1}{2m_N} \left(\overleftarrow{\nabla}_{\mathbf{r}} \times \vec{\sigma}(i)\delta(\mathbf{r} - \mathbf{r}_i) + \delta(\mathbf{r} - \mathbf{r}_i)\vec{\sigma}(i) \times \overrightarrow{\nabla}_{\mathbf{r}} \right) \Bigg\} t_{(i)}^\tau,
\end{aligned} \tag{3.2.12}$$

where $\vec{\sigma}(i)$ refers to the set of three Pauli matrices, acting as spin operators on the ith nucleon, and

$$
\begin{aligned}
\hat{l}_0^\tau &= c_1^\tau + i\hat{\mathbf{S}}_\chi \cdot \left(\frac{\hat{\mathbf{q}}}{m_N} \times \hat{\mathbf{v}}_T^\perp\right) c_5^\tau + \hat{\mathbf{S}}_\chi \cdot \hat{\mathbf{v}}_T^\perp\, c_8^\tau + i\hat{\mathbf{S}}_\chi \cdot \frac{\hat{\mathbf{q}}}{m_N}\, c_{11}^\tau \\
\hat{l}_{0A}^\tau &= -\frac{1}{2}\left(c_7^\tau + i\hat{\mathbf{S}}_\chi \cdot \frac{\hat{\mathbf{q}}}{m_N}\, c_{14}^\tau\right) \\
\hat{\mathbf{l}}_5^\tau &= \frac{1}{2}\Bigg(i\frac{\hat{\mathbf{q}}}{m_N} \times \hat{\mathbf{v}}_T^\perp\, c_3^\tau + \hat{\mathbf{S}}_\chi\, c_4^\tau + \frac{\hat{\mathbf{q}}}{m_N}\hat{\mathbf{S}}_\chi \cdot \frac{\hat{\mathbf{q}}}{m_N}\, c_6^\tau + \hat{\mathbf{v}}_T^\perp\, c_7^\tau + i\frac{\hat{\mathbf{q}}}{m_N} \times \hat{\mathbf{S}}_\chi\, c_9^\tau + i\frac{\hat{\mathbf{q}}}{m_N}\, c_{10}^\tau \\
&\quad + \hat{\mathbf{v}}_T^\perp \times \hat{\mathbf{S}}_\chi\, c_{12}^\tau + i\frac{\hat{\mathbf{q}}}{m_N}\hat{\mathbf{S}}_\chi \cdot \hat{\mathbf{v}}_T^\perp\, c_{13}^\tau + i\hat{\mathbf{v}}_T^\perp\hat{\mathbf{S}}_\chi \cdot \frac{\hat{\mathbf{q}}}{m_N}\, c_{14}^\tau + \frac{\hat{\mathbf{q}}}{m_N} \times \hat{\mathbf{v}}^\perp\hat{\mathbf{S}}_\chi \cdot \frac{\hat{\mathbf{q}}}{m_N}\, c_{15}^\tau\Bigg) \\
\hat{\mathbf{l}}_M^\tau &= i\frac{\hat{\mathbf{q}}}{m_N} \times \hat{\mathbf{S}}_\chi\, c_5^\tau - \hat{\mathbf{S}}_\chi\, c_8^\tau \\
\hat{\mathbf{l}}_E^\tau &= \frac{1}{2}\left(\frac{\hat{\mathbf{q}}}{m_N}\, c_3^\tau + i\hat{\mathbf{S}}_\chi\, c_{12}^\tau - \frac{\hat{\mathbf{q}}}{m_N} \times \hat{\mathbf{S}}_\chi\, c_{13}^\tau - i\frac{\hat{\mathbf{q}}}{m_N}\hat{\mathbf{S}}_\chi \cdot \frac{\hat{\mathbf{q}}}{m_N}\, c_{15}^\tau\right).
\end{aligned}
\tag{3.2.13}
$$

Integrating the Hamiltonian density over all space gives the full Hamiltonian, H_T, which eliminates the delta functions. The scattering amplitude is given by relation

$$
\langle f|H_T|i\rangle = i\mathcal{M}(2\pi)^3\delta(\mathbf{k}'_\mathbf{T} + \mathbf{p}' - \mathbf{k}_\mathbf{T} - \mathbf{p}). \tag{3.2.14}
$$

The initial state is defined by the momentum and quantum numbers of the nucleus, including spin, isospin and their associated magnetic momenta, as well as the momentum, spin and magnetic moment of the WIMP, like

$$
|i\rangle = |\mathbf{k}_T, J, M_J, T, M_T\rangle \otimes |\mathbf{p}, j_\chi, M_\chi\rangle. \tag{3.2.15}
$$

An analogous expression applies for the final state, $\langle f|$.

In order to evaluate the differential cross section, we must square the scattering amplitude and integrate over all free variables. This is a lengthy task and not presented in detail. The end result can be presented like

$$
\begin{aligned}
\frac{\mathrm{d}\sigma}{\mathrm{d}E_R}(w^2,q^2) =& \frac{1}{2j_\chi+1}\frac{1}{2J+1}\frac{m_T}{2\pi w^2}\sum_{\text{spins}}|\mathcal{M}|^2 = \\
=& \frac{1}{2J+1}\frac{2m_T}{w^2}\sum_{\tau}\sum_{\tau'}\Bigg\{R_M^{\tau\tau'}\left(v_T^{\perp 2},\frac{q^2}{m_N^2}\right)W_M^{\tau\tau'}(y) \\
&+ R_{\Sigma''}^{\tau\tau'}\left(v_T^{\perp 2},\frac{q^2}{m_N^2}\right)W_{\Sigma''}^{\tau\tau'}(y) + R_{\Sigma'}^{\tau\tau'}\left(v_T^{\perp 2},\frac{q^2}{m_N^2}\right)W_{\Sigma'}^{\tau\tau'}(y) \\
&+ \frac{q^2}{m_N^2}\Bigg[R_{\Phi''}^{\tau\tau'}\left(v_T^{\perp 2},\frac{q^2}{m_N^2}\right)W_{\Phi''}^{\tau\tau'}(y) + R_{\Phi''M}^{\tau\tau'}\left(v_T^{\perp 2},\frac{q^2}{m_N^2}\right)W_{\Phi''M}^{\tau\tau'}(y) \\
&+ R_{\tilde{\Phi}'}^{\tau\tau'}\left(v_T^{\perp 2},\frac{q^2}{m_N^2}\right)W_{\tilde{\Phi}'}^{\tau\tau'}(y) + R_{\Delta}^{\tau\tau'}\left(v_T^{\perp 2},\frac{q^2}{m_N^2}\right)W_{\Delta}^{\tau\tau'}(y) \\
&+ R_{\Delta\Sigma'}^{\tau\tau'}\left(v_T^{\perp 2},\frac{q^2}{m_N^2}\right)W_{\Delta\Sigma'}^{\tau\tau'}(y)\Bigg]\Bigg\}. \qquad (3.2.16)
\end{aligned}
$$

The quantities denoted $R^{\tau\tau'}$ are the WIMP response functions, quadratic combinations of the various l quantities from equation (3.2.13). The full expressions for the WIMP response functions can be found in table 3.3. The quantities denoted $W^{\tau\tau'}$ are the nuclear response function, which is different for each nuclear isotope. They are polynomial functions times an exponential suppression factor containing quantity $y = (bq/2)^2$. Here q is the transferred momentum and b is the harmonic oscillator length of the nucleus, which is assumed to be $b = \sqrt{41.647/(45A^{-1/3} - 25A^{-2/3})}$.

The nuclear response functions are taken from a paper by Catena and Schwabe [59], which in turn built on Mathematica package for WIMP direct detection [58]. The nuclear response functions were calculated numerically using one-body density matrix elements (OBDME). The OBDMEs are from the `Nushell@MSU` program, which is based on a nuclear shell model. For the calculations in this thesis, a modified version of the Mathematica package for WIMP direct detection has been used. The program provides the differential cross-section, described in equation (3.2.16), as a function of nuclear isotope, WIMP mass and spin, and chosen interaction coefficient values. The package is user friendly and does not necessitate an in-depth understanding of how to derive the response functions. Neither is that the primary focus of this thesis. For further information on the subject, the reader is encouraged to look at the references mentioned above.

$$
\begin{array}{rcl}
R_M^{\tau\tau'} & = & c_1^\tau c_1^{\tau'} + \frac{j_\chi(j_\chi+1)}{3}\left(\frac{q^2}{m_N^2} v_T^{\perp 2} c_5^\tau c_5^{\tau'} + v_T^{\perp 2} c_8^\tau c_8^{\tau'} + \frac{q^2}{m_N^2} c_{11}^\tau c_{11}^{\tau'}\right) \\
R_{\Phi''}^{\tau\tau'} & = & \frac{q^2}{4m_N^2} c_3^\tau c_3^{\tau'} + \frac{j_\chi(j_\chi+1)}{12}\left(c_{12}^\tau - \frac{q^2}{m_N^2} c_{15}^\tau\right)\left(c_{12}^{\tau'} - \frac{q^2}{m_N^2} c_{15}^{\tau'}\right) \\
R_{\Phi'' M}^{\tau\tau'} & = & c_3^\tau c_1^{\tau'} + \frac{j_\chi(j_\chi+1)}{3}\left(c_{12}^\tau - \frac{q^2}{m_N^2} c_{15}^\tau\right) c_{11}^{\tau'} \\
R_{\tilde{\Phi}'}^{\tau\tau'} & = & \frac{j_\chi(j_\chi+1)}{12}\left(c_{12}^\tau c_{12}^{\tau'} + \frac{q^2}{m_N^2} c_{13}^\tau c_{13}^{\tau'}\right) \\
R_{\Sigma''}^{\tau\tau'} & = & \frac{q^2}{4m_N^2} c_{10}^\tau c_{10}^{\tau'} + \frac{j_\chi(j_\chi+1)}{12}\Big[c_4^\tau c_4^{\tau'} + \frac{q^2}{m_N^2}(c_4^\tau c_6^{\tau'} + c_6^\tau c_4^{\tau'}) + \\
 & & + \frac{q^4}{m_N^4} c_6^\tau c_6^{\tau'} + v_T^{\perp 2} c_{12}^\tau c_{12}^{\tau'} + \frac{q^2}{m_N^2} v_T^{\perp 2} c_{14}^\tau c_{14}^{\tau'}\Big] \\
R_{\Sigma'}^{\tau\tau'} & = & \frac{1}{8}\left(\frac{q^2}{m_N^2} v_T^{\perp 2} c_3^\tau c_3^{\tau'} + v_T^{\perp 2} c_7^\tau c_7^{\tau'}\right) + \frac{j_\chi(j_\chi+1)}{12}\Big[c_4^\tau c_4^{\tau'} + \frac{q^2}{m_N^2} c_9^\tau c_9^{\tau'} + \\
 & & + \frac{v_T^{\perp 2}}{2}\left(c_{12}^\tau - \frac{q^2}{m_N^2} c_{15}^\tau\right)\left(c_{12}^{\tau'} - \frac{q^2}{m_N^2} c_{15}^{\tau'} + \frac{q^2}{2m_N^2} v_T^{\perp 2} c_{14}^\tau c_{14}^{\tau'}\right)\Big] \\
R_{\Delta}^{\tau\tau'} & = & \frac{j_\chi(j_\chi+1)}{3}\left(\frac{q^2}{m_N^2} c_5^\tau c_5^{\tau'} + c_8^\tau c_8^{\tau'}\right) \\
R_{\Delta\Sigma'}^{\tau\tau'} & = & \frac{j_\chi(j_\chi+1)}{3}\left(c_5^\tau c_4^{\tau'} - c_8^\tau c_9^{\tau'}\right)
\end{array}
$$

Table 3.3: WIMP response functions.

3.2.3 WIMP self-interaction

In the case of WIMP self-interaction, everything works in complete analogy with WIMP-proton interaction. The WIMPs are assumed to have spin 1/2, as hydrogen does. The nuclear response functions in the expression for the differential cross-section, equation (3.2.16), simply uses the values for hydrogen,

$$
\begin{aligned}
W_M^{\mathrm{WIMP}} &= \frac{1}{8\pi} \\
W_{\Sigma''}^{\mathrm{WIMP}} &= \frac{1}{8\pi} \\
W_{\Sigma'}^{\mathrm{WIMP}} &= \frac{1}{4\pi}.
\end{aligned}
\tag{3.2.17}
$$

The other W's are zero, as they account for a nucleus' sub-structure. The total differential cross-section for WIMP self-interaction becomes

$$
\frac{\mathrm{d}\sigma_{\chi\chi}}{\mathrm{d}E_R}(w^2, q^2) = \tag{3.2.18}
$$

$$
\frac{m_T}{w^2}\left[R_M\left(v_T^{\perp 2}, \frac{q^2}{m_N^2}\right)\frac{1}{8\pi} + R_{\Sigma''}\left(v_T^{\perp 2}, \frac{q^2}{m_N^2}\right)\frac{1}{8\pi} + R_{\Sigma'}\left(v_T^{\perp 2}, \frac{q^2}{m_N^2}\right)\frac{1}{4\pi}\right].
$$

The indices τ and τ', representing isoscalar and isovector couplings, are of course dropped. Apart from that the WIMP response functions, denoted R, remain the same, as in table 3.3.

3.3 Interaction coefficient limits

The aim of this thesis is to find out whether the WIMP self-interaction can make a significant contribution to the number of WIMPs captured by the Sun and the resulting flux of neutrinos. This is done by exploring the parameter space that governs WIMP-nuclei interaction and WIMP self-interaction. Apart from the mass, spin and annihilation coefficient of the hypothesized WIMP, the degrees of freedom lie in the interaction coupling constants, c_i. As described in section 3.2, the coupling constants determine the strength of 14 different interaction operators, $\hat{\mathcal{O}}_i$. In the case of WIMP-nuclei interaction the degrees of freedom is doubled due to isoscalar/isovector (or proton/neutron) couplings. This gives 28 degrees of freedom for the WIMP-nuclei interaction, and 14 degrees of freedom for the WIMP self-interaction.

This parameter space is limited by experiment, theoretical argument, observation, and simulation. The WIMP-nuclei interaction coupling constants have upper bounds, for which the strongest limits come from direct detection experiments. The WIMP self-interaction coupling constants have approximate upper limits coming from galaxy clusters, as well as some astronomical arguments for a lower limit.

3.3.1 Limits for WIMP-nuclei interaction

The limits used for the WIMP-nuclei isoscalar and isovector coupling constants, c_i^0 and c_i^1, are taken directly from an article by Catena [57]. Figure 3.2 shows the limits for coupling constant c_1^0. As seen in the figure, the strongest limit on the coupling constant is for a mass of ~ 50 GeV. This is due to the particle mass of the LUX detector medium, which is xenon with mass number 54.

The LUX experiment provides the strongest limit over the whole mass range (10–1000 GeV) for almost all 28 coupling constants. The most notable exception is the case of c_7^0, for which the limit provided by IceCUBE is actually one order of magnitude stronger. However, these limits are derived from the hypothesized but not yet detected neutrino signal from the Sun, produced by WIMP annihilation (without including self-interaction in the description). The limits are set under the assumption of certain annihilation channels. For what is called the *soft* case in figure 3.2, represented by a dashed line, the WIMPs are assumed to annihilate into a $b\bar{b}$ quark pair. For the *hard* case, represented by a solid line, the annihilation

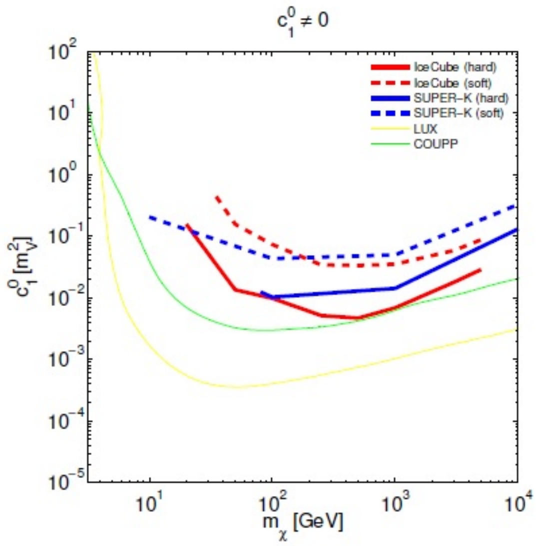

Figure 3.2: An image from an article by Catena [57], showing the limits on coupling constant c_1^0. The strongest limit comes from the LUX detector, represented in yellow. The vertical axis scale is with respect to the Higgs field vacuum expectation value, $m_v = 246.2$ GeV.

product is assumed to a W^+W^- pair. For the calculations and analysis in this thesis, only the limits provided by the LUX direct detection experiment are used.

3.3.2 Limits for WIMP self-interaction

The strength of dark matter self-interaction is a hot topic of debate. While non-collisional cold dark matter has been proved very successful in explaining large-scale cosmological behavior, some smaller-scale phenomena are more problematic in such a theory. Simulations of collisionless cold dark matter at galaxy to galaxy cluster scales predict more centrally concentrated halo densities [7] and more halo substructure [60] than what is observed. This is known as the *cuspy halo problem.*

Various solutions to this problem has been proposed. For example, violent astrophysical processes such as supernovae could affect the halo structure by heat dissipation, caused by rapid fluctuations of the gravitational potential [11]. Another solution could be that dark matter is not cold, but has a higher velocity. The idea relevant to this thesis is that dark matter is self-interacting [8]. Estimates of the strength of such self-interaction vary, and consensus on the issue has not been reached.

A recent study of halo substructure in galaxy to galaxy cluster scales [9] found that a constant total cross-section of $\sigma_{\chi\chi} \simeq 0.1 \, \frac{M_\chi}{\mathrm{g}} \, \mathrm{cm}^2$ is capable of reproducing the observed density distribution shapes. Their simulations also suggests that no velocity dependence in the total cross-section is necessary, at least not in the regime of the typical collisional velocity at these scales, in the approximative range of 20–1000 km/s. The lower value comes from dwarf galaxies and the higher value from galaxy clusters. A similar study on dwarf spheroidals around the Milky Way [10] reaches a similar result in the approximate range of 0.1–1 $\frac{M_\chi}{\mathrm{g}} \, \mathrm{cm}^2$.

However, there is some tension with other results. A recent study of a galaxy falling into the core of a galaxy cluster [61] has produced a higher estimate of $\sigma_{\chi\chi} \simeq 1.5 \, \frac{M_\chi}{\mathrm{g}} \, \mathrm{cm}^2$. In this case, the merger velocity is $\sim$ 1500 km/s. Conversely, an somewhat older study [62] examined the ellipticity properties of a galaxy cluster and found a significantly lower total cross-section of $\sim 0.02 \, \frac{M_\chi}{\mathrm{g}} \, \mathrm{cm}^2$.

In this thesis, the limit I use for the WIMP self-interaction cross-section used is

$$\sigma_{\chi\chi} < 0.1 \, \frac{M_\chi}{\mathrm{g}} \, \mathrm{cm}^2 = 1.78 \cdot 10^{-25} \, \frac{M_\chi}{\mathrm{GeV}} \, \mathrm{cm}^2. \tag{3.3.1}$$

For the operators that have a dependence on collisional velocity, I assume that the cross-section is evaluated for $v = 1000$ km/s. This is the conservative choice, as it sets the strictest limit for cross-sections of higher collisional velocity (recall that the escape velocity from the Sun's core is 1380 km/s).

Another upper limit for WIMP self-interactions, that is perhaps more credible and definite, is provided by the Bullet Cluster, previously discussed in section 2.1. With combined information from X-ray and optical observation, strong and weak gravitational lensing and numerical simulation, the merging galaxy cluster has placed an upper limit (68 % confidence) of

$$\sigma_{\chi\chi} < 1.25 \, \frac{M_\chi}{\mathrm{g}} \, \mathrm{cm}^2 = 2.23 \cdot 10^{-24} \, \frac{M_\chi}{\mathrm{GeV}} \, \mathrm{cm}^2. \tag{3.3.2}$$

If it is assumed that the two merging clusters had equal mass-to-light ratios prior to collision, the constraint can be made stronger, to $0.7 \, \frac{M_\chi}{\mathrm{g}} \, \mathrm{cm}^2$. The less restrictive limit, not dependent on this assumption, is used in this thesis.

On a side note, a similar but more extensive study has provided a stronger limit to the constant cross-section [63] than what was set by the Bullet Cluster. A total of 72 cluster collisions was used in the analysis. The limit found was $0.47 \cdot 10^{-24} \, \frac{M_\chi}{\mathrm{g}} \, \mathrm{cm}^2$ (95 % confidence). This limit is not used in this thesis, however. Most of the cluster collisions have roughly the same collisional velocity as the limit in equation (3.3.1), which is more stringent. The Bullet Cluster, on the other hand, is a case of exceptionally high collisional velocity compared to other merging clusters, which is why it still provides a stronger limit for the operators with a quadratic or cubic dependence on transferred momentum.

The constant cross-section corresponds to operator $\hat{\mathcal{O}}_1 = \mathbb{1}_{\chi\chi}$ or $\hat{\mathcal{O}}_4 = \hat{\mathbf{S}}_\chi \cdot \hat{\mathbf{S}}_N$. Thus the upper limit for coupling constants c_1 and c_4 are trivially found. The other coupling constants have a dependence on transferred momentum, which makes the cross-section vary with collisional velocity. In order to find the limits to their corresponding coupling constants, I calculate the total cross-sections for the typical collisional velocity of the limit in question. For the limit provided by cluster simulations I use a collisional velocity of 1000 km/s and for the Bullet Cluster the merger velocity is 4700 km/s. Which one of these two limits that is the strongest depends on the operator.

It has been considered that the calculations of total cross-section for the different operators should have some integrand weight. For example, interactions for which the momentum transfer is very low could be given less significance, as they have a weaker and less visible effect on a cluster merger. The total cross-section, written like an integral over scattering angle with an added integrand weight, $W(\cos\theta)$, looks like

$$\sigma_{\chi\chi} = \int_0^1 \frac{\mathrm{d}\sigma_{\chi\chi}}{\mathrm{d}E_r}\,(v,E_r(\cos\theta))\,\frac{\mathrm{d}E_r}{\mathrm{d}(\cos\theta)} W(\cos\theta)\mathrm{d}(\cos\theta). \tag{3.3.3}$$

A weight that was considered was $W \propto \cos\theta(1-\cos\theta)$: one factor $\cos\theta$ because it is proportional to the transferred momentum and one factor $(1-\cos\theta)$ because scattering to the side is what causes dissipation of the colliding halos. The most dramatic effect is on operator $\hat{\mathcal{O}}_{15}$, whose coupling constant limit coming from the Bullet Cluster is made *less restrictive* by a factor 1.7 relative to the case without integrand weight. In the end, using such a weight was decided against. Exactly how the analysis of the Bullet Cluster [64] was made is not known which makes it difficult to choose the correct weight; furthermore, this is an order-of-magnitude argument and the conclusions drawn in this thesis are not contingent on this specific numerical adjustments.

3.4 Capture rate differential equations

In this section I present and discuss the differential equations that describe the WIMP capture and annihilation processes and how the concentration of trapped WIMPs within the Sun changes over time. I also define a quantity β, which is the relative amplification of the neutrino flux, due to WIMP self-interaction.

I begin with the case of no WIMP self-interaction, for which the differential equation looks like

$$\frac{\mathrm{d}N}{\mathrm{d}t} = C_c - C_a N^2. \tag{3.4.1}$$

Here, N is the number of captured WIMPs, C_c is the rate of capture by nuclei and C_a is the annihilation rate. The term that accounts for annihilation contains N^2, as it is proportional to the number of possible pairs of captured WIMPs. Solving this equation gives

$$\begin{aligned}
\frac{\mathrm{d}N}{\mathrm{d}t} &= C_c\left(1-\frac{C_a}{C_c}N^2\right) \\
\left(1-\frac{C_a}{C_c}N^2\right)^{-1}\frac{\mathrm{d}N}{\mathrm{d}t} &= C_c \\
\sqrt{\frac{C_c}{C_a}}\frac{\mathrm{d}}{\mathrm{d}t}\left[\tanh^{-1}(\sqrt{\frac{C_a}{C_c}}N)\right] &= C_c \\
\frac{\mathrm{d}}{\mathrm{d}t}\left[\tanh^{-1}(\sqrt{\frac{C_a}{C_c}}N)\right] &= \sqrt{C_cC_a} \\
\tanh^{-1}(\sqrt{\frac{C_a}{C_c}}N) &= \sqrt{C_cC_a}t+\text{const.} \\
N &= \sqrt{\frac{C_c}{C_a}}\tanh\left(\sqrt{C_cC_a}t+\text{const.}\right).
\end{aligned} \tag{3.4.2}$$

Choosing an initial condition, $N(t=0)=0$, determines the value of the constant in the above expression, such that

$$N=\sqrt{\frac{C_c}{C_a}}\tanh\left(\sqrt{C_cC_a}t\right). \tag{3.4.3}$$

In the limit where $t\to\infty$, the number of captured WIMPs reaches an equilibrium, $N_{eq}=\sqrt{C_c/C_a}$.

In the case of also including WIMP self-interaction, the differential equation gets an additional term, like

$$\frac{\mathrm{d}N}{\mathrm{d}t}=C_c+C_sN-C_aN^2, \tag{3.4.4}$$

where C_s is the capture rate via self-interaction.

For shorthand I use a definition from an article by Zentner [1],

$$\zeta=\frac{1}{\sqrt{C_cC_a+C_s^2/4}}. \tag{3.4.5}$$

The differential equation (3.4.4) can be solved like

$$
\begin{aligned}
\frac{dN}{dt} &= \left(C_c + \frac{C_s^2}{4C_a}\right)\left(1 - \frac{C_a}{C_c + \frac{C_s^2}{4C_a}}(N - \frac{C_s}{2C_a})^2\right)\\
\frac{dN}{dt} &= \frac{1}{C_a\zeta^2}\left(1 - C_a^2\zeta^2(N - \frac{C_s}{2C_a})^2\right)\\
\frac{1}{1 - C_a^2\zeta^2(N - \frac{C_s}{2C_a})^2}\frac{dN}{dt} &= \frac{1}{C_a\zeta^2}\\
\frac{1}{C_a\zeta}\frac{d}{dt}\left[\tanh^{-1}\left(C_a\zeta(N - \frac{C_s}{2C_a})\right)\right] &= \frac{1}{C_a\zeta^2}\\
\tanh^{-1}\left(C_a\zeta(N - \frac{C_s}{2C_a})\right) &= t/\zeta + \text{const.}\\
N &= \frac{1}{C_a\zeta}\tanh\left(t/\zeta + \text{const.}\right) + \frac{C_s}{2C_a}.
\end{aligned} \tag{3.4.6}
$$

The initial condition $N(t = 0) = 0$ sets

$$
\text{const.} = \tanh^{-1}\left(-\frac{C_s\zeta}{2}\right). \tag{3.4.7}
$$

To rewrite the solution further, I use identity

$$
\tanh(a + b) = \frac{\tanh a + \tanh b}{1 + \tanh a \tanh b}, \tag{3.4.8}
$$

which gives me

$$
\begin{aligned}
N &= \frac{\tanh(t/\zeta) - C_s\zeta/2}{C_a\zeta(1 - C_s\zeta\tanh(t/\zeta)/2)} + \frac{C_s}{2C_a} =\\
&= \frac{\tanh(t/\zeta) - C_s\zeta/2 + C_s\zeta/2 - C_s^2\zeta^2\tanh(t/\zeta)/4}{C_a\zeta(1 - C_s\zeta\tanh(t/\zeta)/2)} =\\
&= \frac{(1 - C_s^2\zeta^2/4)\tanh(t/\zeta)}{C_a\zeta(1 - C_s\zeta\tanh(t/\zeta)/2)} =\\
&= \frac{1 - C_s^2\zeta^2/4}{C_a\zeta}\,\frac{\tanh(t/\zeta)}{\zeta^{-1} - C_s\tanh(t/\zeta)/2} =\\
&= \frac{C_c\tanh(t/\zeta)}{\zeta^{-1} - C_s\tanh(t/\zeta)/2}.
\end{aligned} \tag{3.4.9}
$$

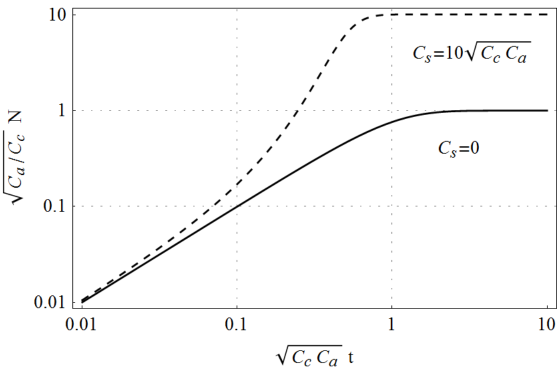

Figure 3.3: An example of how the total amount of trapped WIMPs, N, changes over time, t. Both axes are normalized and in logarithmic scale. The solid line represents the case of no self-interaction, $C_s = 0$. The dashed line represents the case of strong self-interaction, such that $C_s = 10\sqrt{C_c C_a}$.

In the limit $t \to \infty$, this approaches an equilibrium,

$$N_{eq} = \frac{C_c}{\zeta^{-1} - C_s/2} = \frac{C_s}{2C_a} + \sqrt{\frac{C_c}{C_a} + \frac{C_s^2}{4C_a^2}}. \tag{3.4.10}$$

If $C_s^2 > C_c C_a$, self-capture becomes the dominant capture process at the equilibrium steady state. Visible in figure 3.3 is an illustration of how the amount of trapped WIMPs changes over time and how the resulting equilibrium state depend on the relative strength of self-interaction.

The annihilation rate, the number of annihiliation events per unit time, at equilibrium is

$$\Gamma_a = \frac{1}{2} C_a N_{eq}^2, \tag{3.4.11}$$

where the factor 1/2 is due to one event annihilating two WIMPs. From this I can define a quantity β, which is the relative amplification of the annihilation rate and of the produced neutrino flux, for the case of having or not having a WIMP self-interaction,

$$\begin{aligned} \beta &= \left(\frac{N_{C_s \neq 0}(t)}{N_{C_s=0}(t)}\right)^2 \\ &= \left(\frac{\sqrt{C_c C_a}\coth(\sqrt{C_c C_a}t)\tanh(t/\zeta)}{\zeta^{-1} - C_s \tanh(t/\zeta)/2}\right)^2. \end{aligned} \tag{3.4.12}$$

We can note in this expression that the parameters C_c and C_a only occur as a product (also in quantity ζ). This means that the relative amplification is unaffected if C_c is increased and C_a is decreased by the same factor. In the equilibrium case, as $t \to \infty$, the amplification factor becomes

$$\beta_{eq} = \frac{C_s^2}{2C_cC_a} + \sqrt{\left(\frac{C_s^2}{2C_cC_a}\right)^2 + 1}. \tag{3.4.13}$$

In the case of WIMP self-capture being the dominant process, the amplification factor becomes $\beta \simeq C_s^2/(C_cC_a)$. In the other limit, where self-capture is weak, the amplification tends to $\beta \simeq 1 + C_s^2/(2C_cC_a)$, where the last term of the expression is small relative to 1.

A final thing worth discussing is the behaviour very early in time, when the solution is far from being equilibrized. In this case the concentration of captured WIMPs is not yet high enough for annihilation to have significant effect. By neglecting annihilation, C_a, the differential equation looks like

$$\frac{\mathrm{d}N}{\mathrm{d}t} = C_c + C_sN. \tag{3.4.14}$$

Given the initial condition $N(t = 0) = 0$, this has solution

$$N = \frac{C_c}{C_s}(e^{C_st} - 1). \tag{3.4.15}$$

In the case where $C_s = 0$, the solution is simply $N = C_ct$. The amplification factor in the non-equilibrized region becomes

$$\beta = \left(\frac{e^{C_st} - 1}{C_st}\right)^2. \tag{3.4.16}$$

Here, the relative amplification factor has no depedence on C_c at all, and will not until significant annihilation comes into effect. Keep in mind that while C_c does not affect the *relative* amplification in the unequilibrized region, it very much affects the absolute rate of capture, the absolute flux of neutrinos and the point in time when equilibration happens.

4

Results

In this chapter, I present the results for the total capture rate and the potential amplification of the neutrino signal. The term *amplification* refers to the relative enhancement of the neutrino signal that comes from including self-interaction in the description, as described in section 3.4.

For the galactic WIMP halo in the solar neighbourhood, I use the following values. The Sun moves with speed $v_\odot = 220$ km/s through the halo. The halo has density 0.4 GeV/cm^3 and velocity dispersion $\bar{v} = 270$ km/s. The WIMPs are assumed to have spin 1/2 and mass in the range of 10–1000 GeV.

4.1 Capture rates by nuclei

The WIMP capture rate by nuclei, what is written C_c in section 3.4, is calculated numerically with equations (3.1.19), (3.1.20), (3.1.21). The 16 most abundant isotopes in the Sun are considered, as presented in table 3.1. The differential cross-sections are taken from a modified version of the direct detection Mathematica package [58], with nuclear response functions from Catena and Schwabe [59].

The capture rates of the 28 WIMP-nuclei interaction operators are visible in figures 4.1–4.5. In these figures, following the convention of Catena and Schwabe [59], the non-zero coupling constant takes on the reference value $c_i^\tau = 10^{-3}\ m_v^{-2}$, where $m_v = 246.2$ GeV is the Higgs field vacuum expectation value.

See table 4.1 for the total capture rates of the 28 WIMP-nuclei interaction operators, evaluated at the interaction strength limit provided by LUX [57] and assuming a WIMP mass of 100 GeV. The total capture rates, C_c, are in the range of 10^{18}–10^{25} s^{-1}. In the low end of the mass spectrum, ~ 10 GeV, C_c is around three orders of magnitude larger. In the high end of the mass spectrum, ~ 1000

Operator	Isoscalar capture rate	Isovector capture rate
1	$1.52 \cdot 10^{20}$ s^{-1}	$1.64 \cdot 10^{19}$ s^{-1}
3	$1.27 \cdot 10^{21}$ s^{-1}	$6.30 \cdot 10^{20}$ s^{-1}
4	$7.54 \cdot 10^{22}$ s^{-1}	$7.91 \cdot 10^{22}$ s^{-1}
5	$1.85 \cdot 10^{21}$ s^{-1}	$1.14 \cdot 10^{21}$ s^{-1}
6	$1.33 \cdot 10^{22}$ s^{-1}	$3.18 \cdot 10^{21}$ s^{-1}
7	$7.54 \cdot 10^{24}$ s^{-1}	$4.05 \cdot 10^{23}$ s^{-1}
8	$1.43 \cdot 10^{21}$ s^{-1}	$2.29 \cdot 10^{20}$ s^{-1}
9	$6.00 \cdot 10^{21}$ s^{-1}	$1.69 \cdot 10^{21}$ s^{-1}
10	$5.89 \cdot 10^{21}$ s^{-1}	$1.43 \cdot 10^{21}$ s^{-1}
11	$2.45 \cdot 10^{20}$ s^{-1}	$4.71 \cdot 10^{18}$ s^{-1}
12	$4.29 \cdot 10^{20}$ s^{-1}	$1.77 \cdot 10^{20}$ s^{-1}
13	$7.76 \cdot 10^{20}$ s^{-1}	$5.60 \cdot 10^{20}$ s^{-1}
14	$4.61 \cdot 10^{22}$ s^{-1}	$6.67 \cdot 10^{21}$ s^{-1}
15	$4.60 \cdot 10^{21}$ s^{-1}	$3.05 \cdot 10^{21}$ s^{-1}

Table 4.1: Maximum total capture rates, C_c, for the 14 operators $\hat{\mathcal{O}}_i$ under isoscalar and isovector coupling, under assumption of $M_\chi = 100$ GeV. The capture rates are calculated for coupling constants, c_i^τ, at values at the upper limit provided by LUX (see section 3.3.1).

GeV, C_c is around one order of magnitude smaller. This mass dependence of C_c is due to the following: the amount of WIMPs in the halo is inversely proportional to the WIMP mass; the lighter WIMPs have resonance effects when colliding with nuclei of similar mass and cross-section decreases like M_χ^{-2} for very mismatched masses; the LUX limit differs somewhat for different masses (see figure 3.2).

The isotope that contributes the most to the total WIMP capture varies with interaction operator and, to a lesser extent, with WIMP mass. Depending on the choice of parameters, the dominant isotope is H, ^{4}He, ^{14}N, ^{16}O, ^{27}Al, ^{56}Fe, or ^{59}Ni. For some operators the heavier nuclei are the most important, especially for operators with a quadratic or cubic dependence on transferred momentum.

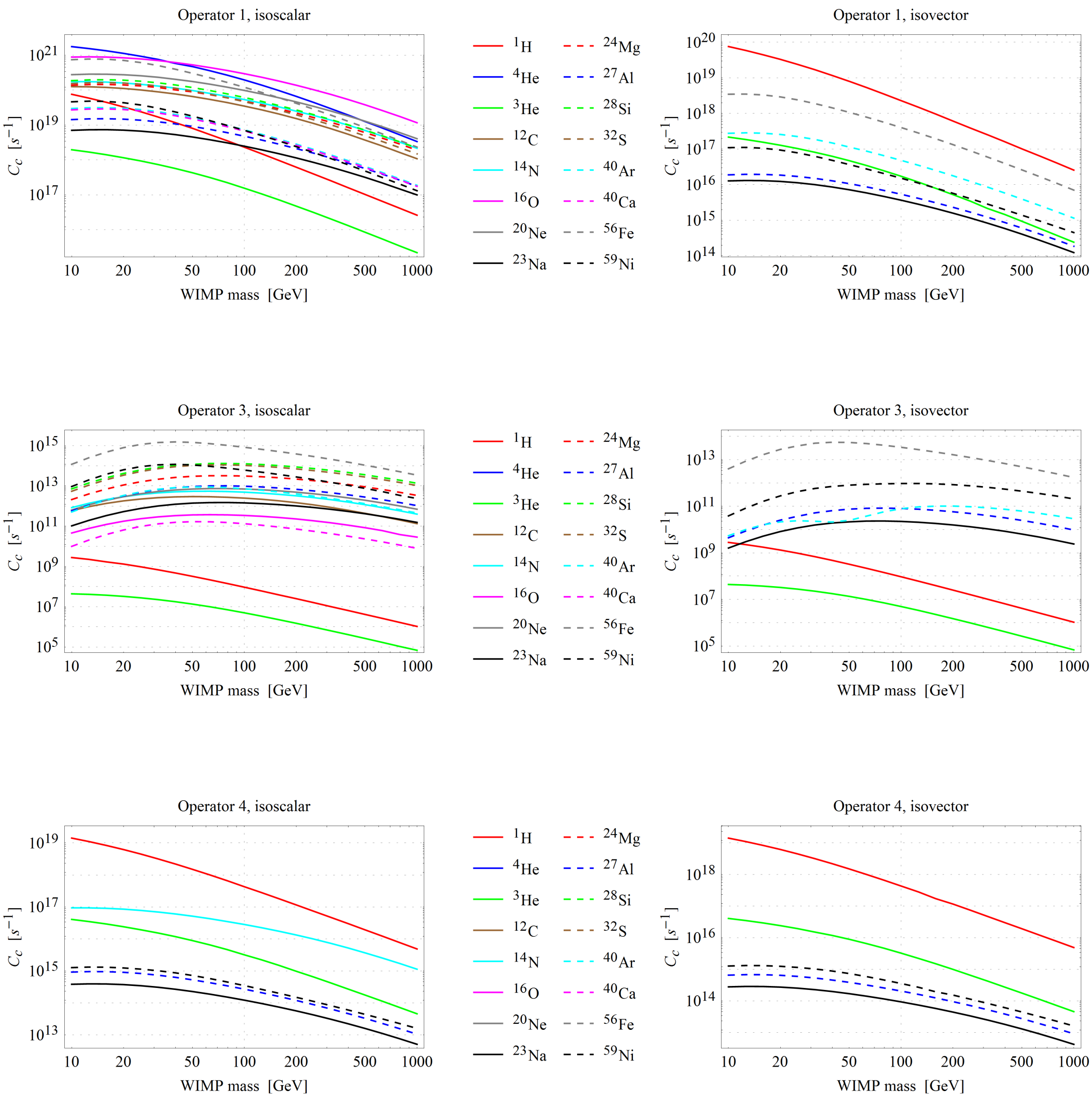

Figure 4.1: Capture rates for WIMP-nuclei interaction, operators $\hat{\mathcal{O}}_1$, $\hat{\mathcal{O}}_3$ and $\hat{\mathcal{O}}_4$, isovector and isoscalar. The coupling constant takes reference value $c_i^\tau = 10^{-3}\ m_v^{-2}$, where $m_v = 246.2$ GeV.

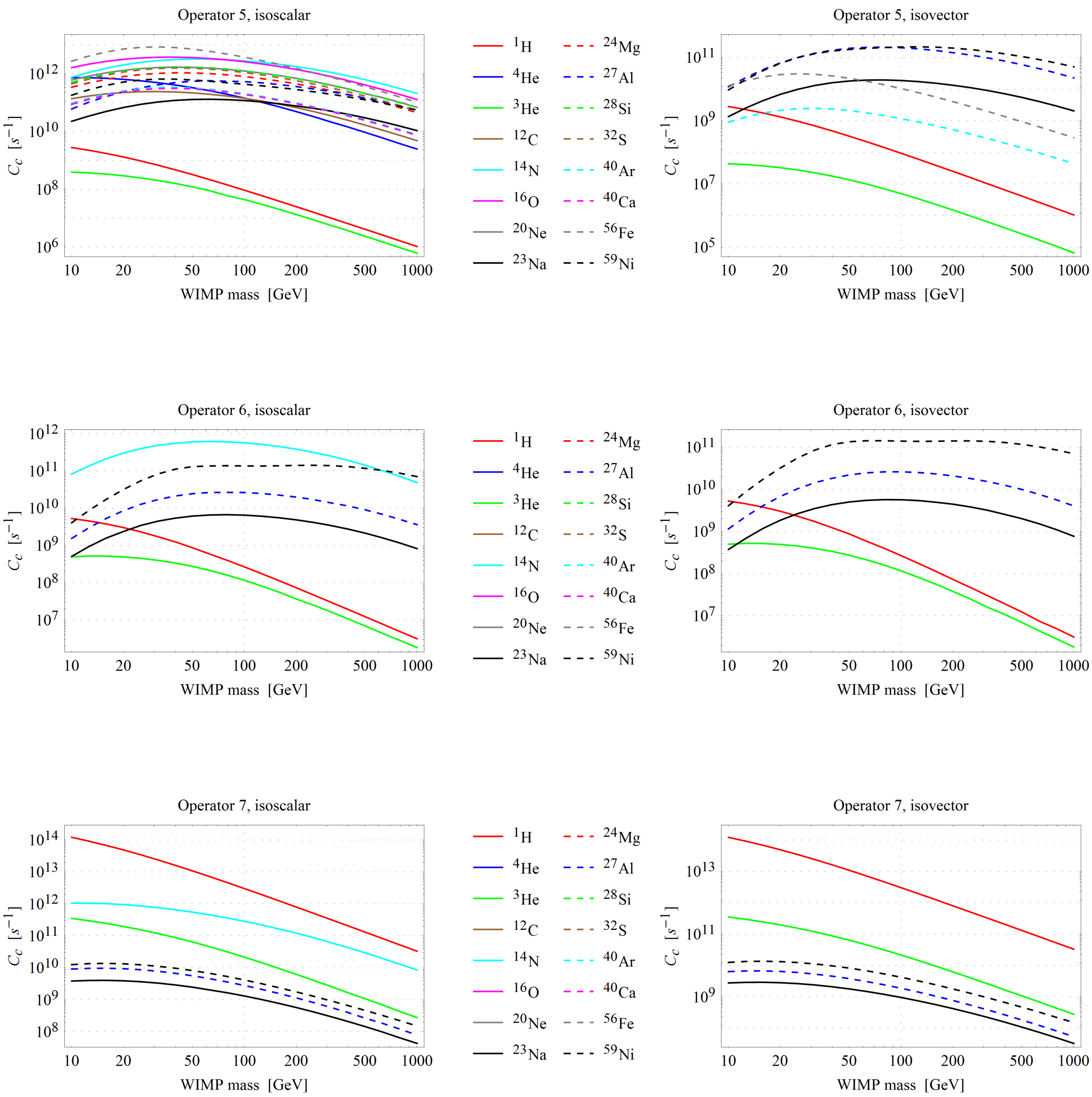

Figure 4.2: Capture rates for WIMP-nuclei interaction, operators $\hat{\mathcal{O}}_5$, $\hat{\mathcal{O}}_6$ and $\hat{\mathcal{O}}_7$, isovector and isoscalar. The coupling constant takes reference value $c_i^{\tau} = 10^{-3}\ m_v^{-2}$, where $m_v = 246.2$ GeV.

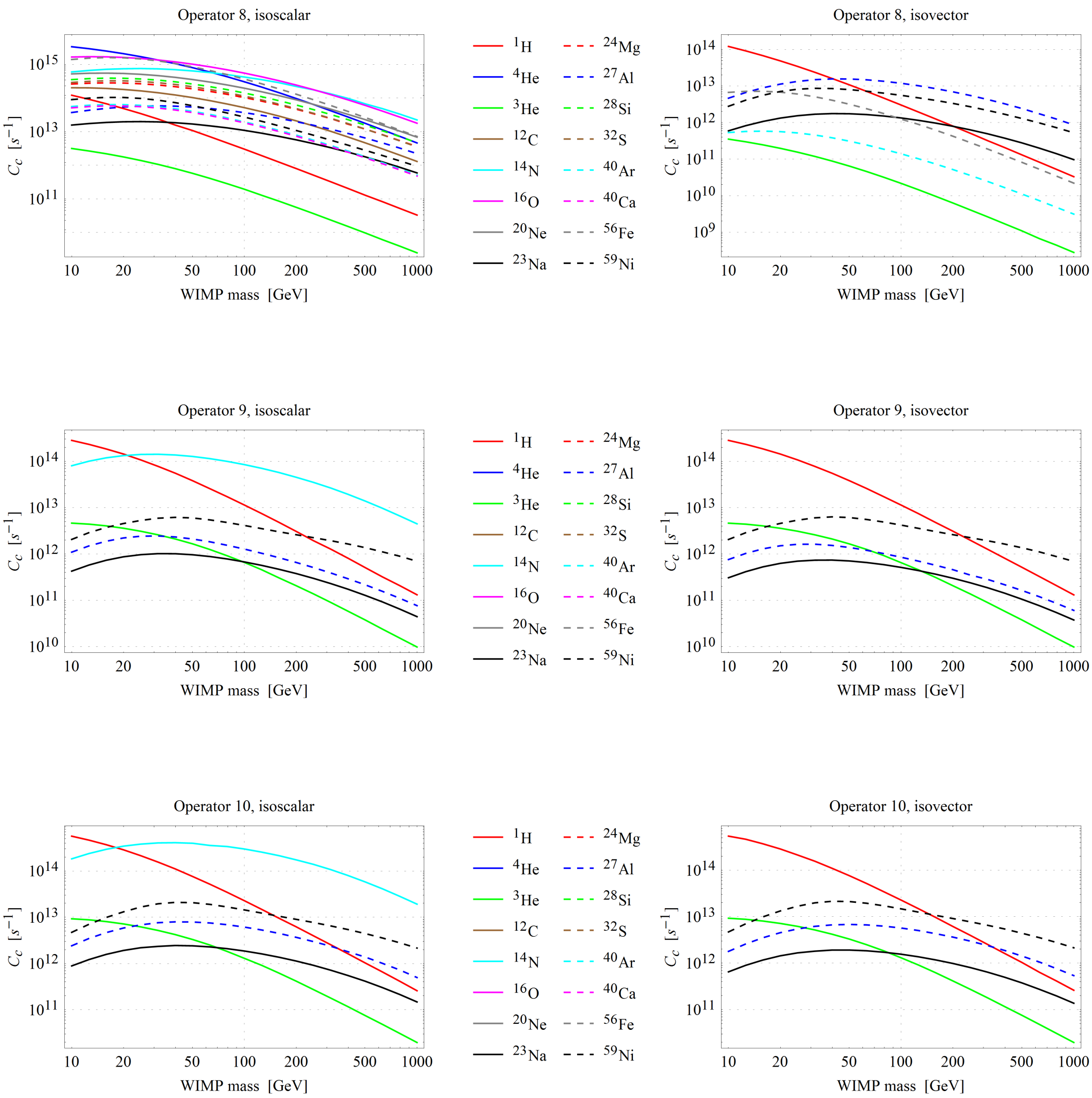

Figure 4.3: Capture rates for WIMP-nuclei interaction, operators $\hat{\mathcal{O}}_8$, $\hat{\mathcal{O}}_9$ and $\hat{\mathcal{O}}_{10}$, isovector and isoscalar. The coupling constant takes reference value $c_i^\tau = 10^{-3}\ m_v^{-2}$, where $m_v = 246.2$ GeV.

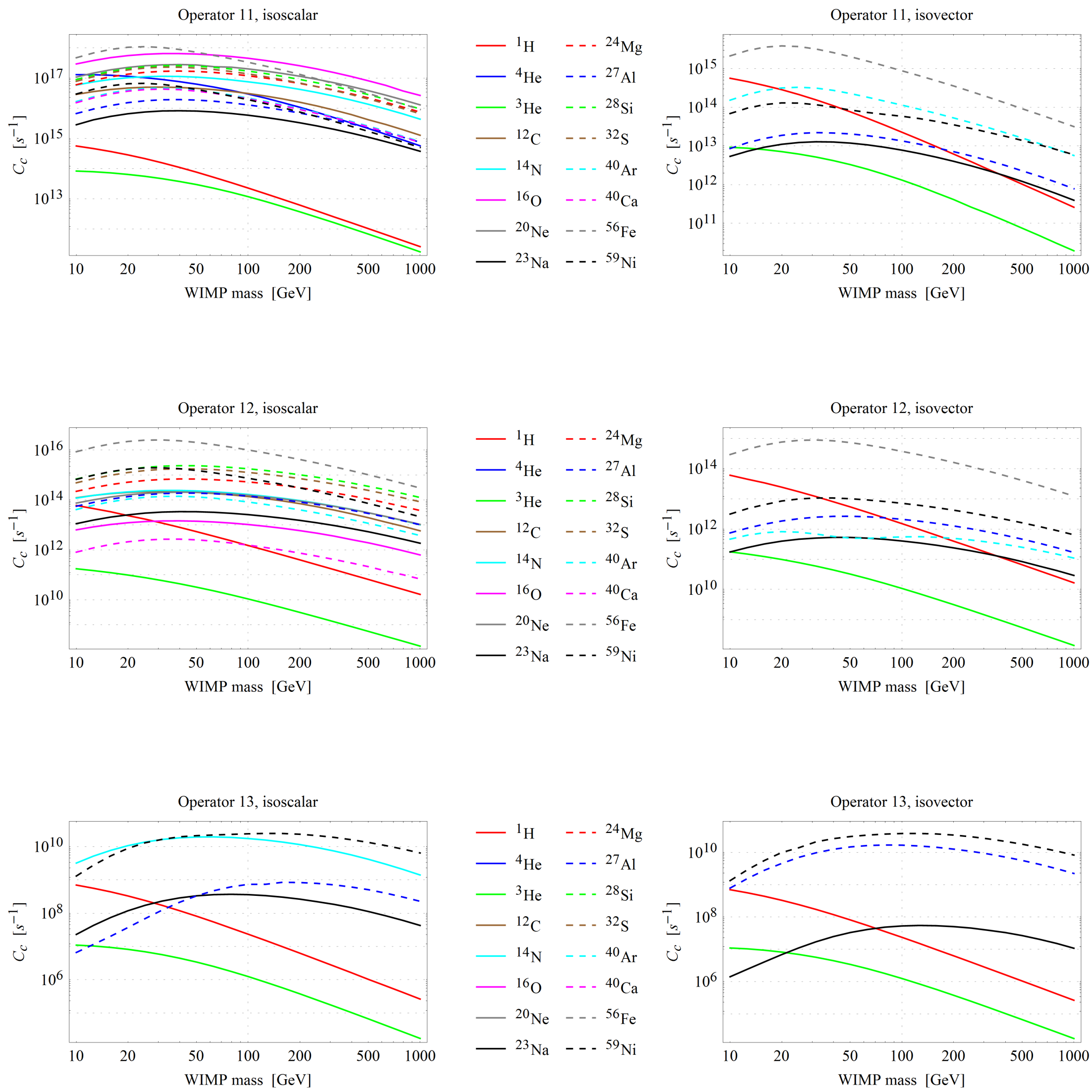

Figure 4.4: Capture rates for WIMP-nuclei interaction, operators $\hat{\mathcal{O}}_{11}$, $\hat{\mathcal{O}}_{12}$ and $\hat{\mathcal{O}}_{13}$, isovector and isoscalar. The coupling constant takes reference value $c_i^\tau = 10^{-3}$ m_v^{-2}, where $m_v = 246.2$ GeV.

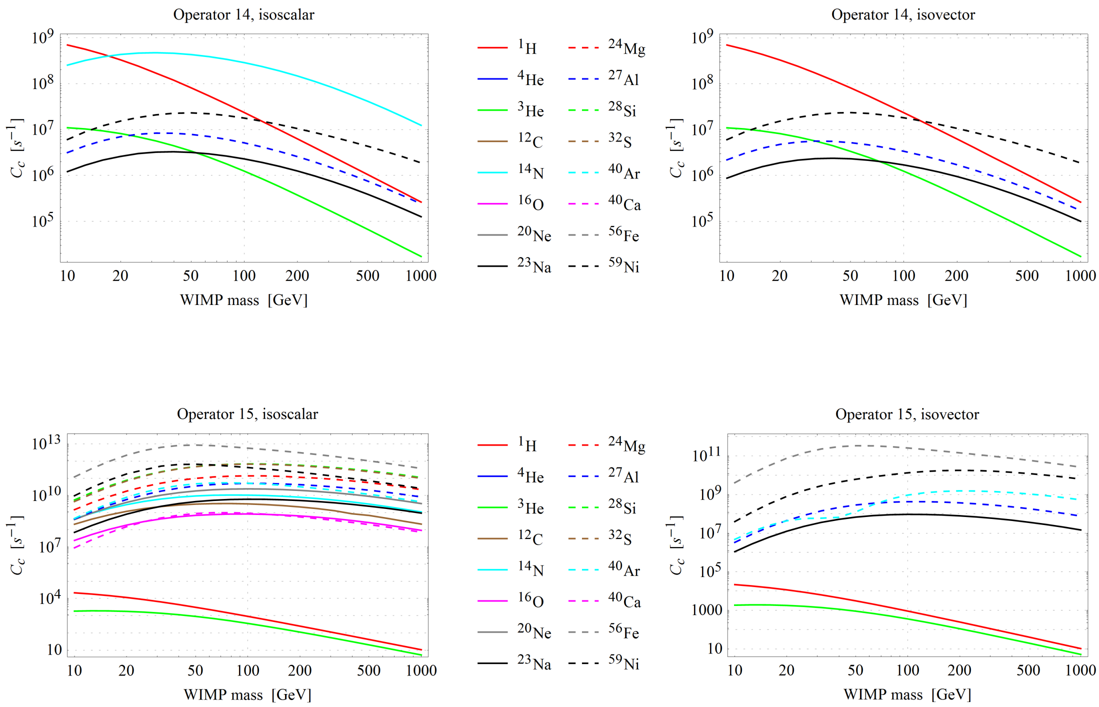

Figure 4.5: Capture rates for WIMP-nuclei interaction, operators $\hat{\mathcal{O}}_{14}$ and $\hat{\mathcal{O}}_{15}$, isovector and isoscalar. The coupling constant takes reference value $c_i^\tau = 10^{-3}\ m_v^{-2}$, where $m_v = 246.2$ GeV.

4.2 Capture rates by self-interaction

This section is about the WIMP capture rate due to WIMP self-interaction, what is written C_s in section 3.4. This capture rate is calculated very much like for WIMP-nuclei interactions, but with differences described in section 3.1.5.

In figure 4.6 the self-capture rates for the 14 different types of WIMP self-interaction are visible. In the figure, the coupling constants are set such that the total cross-section is precisely on the limit provided by galaxy cluster simulations [9]: $\sigma(v = 1000\text{km/s}) = 1.78 \cdot 10^{-25}\ \frac{M_\chi}{\text{GeV}}\ \text{cm}^2$. They fall into four very distinct groups, depending on the power of transferred momentum in the interaction operator. The reason for this splitting is that the trapped WIMPs are localized in the core of the Sun, where the escape velocity is ~ 1380 km/s. This velocity is higher than the typical collisional velocity of the cross-section limit, which is 1000 km/s. Hence the operators that have a higher power of transferred momentum have higher capture rates. The reason why the capture rates are smaller in the

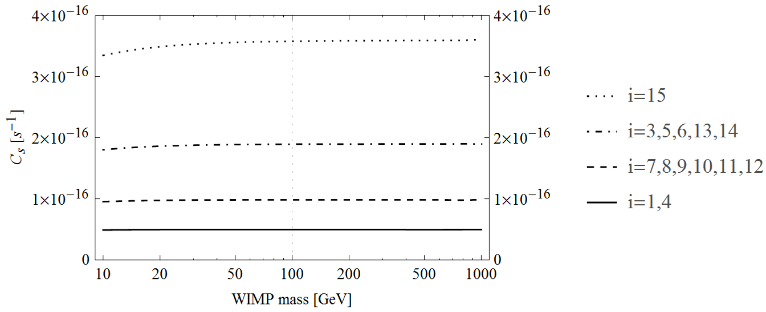

Figure 4.6: Self-capture rates, C_s, for the different operators, $\mathcal{O}_i$. The coupling constants are set such that they fulfill that $\sigma(v = 1000\text{km/s}) = 1.78 \cdot 10^{-25} \frac{M_\chi}{\text{GeV}}$. The operators represented by the same graph line differ in C_s by less than 3 %.

low mass range is that low mass WIMPs are less localized in the Sun's core, which lowers the average collisional velocity.

While this is the case for the limit provided at collisional velocity 1000 km/s, the opposite is true for the limit provided by the Bullet Cluster [64], as described in section 3.3.2. The typical collisional velocity for this event was 4700 km/s, which is significantly higher than the collisional velocity for WIMP capture by the Sun. This limit is the most restrictive for the operators with a high power of transferred momentum. This gives the effect that the stronger limit is provided by different sources. For the operators with no dependence on transferred momentum, the strongest limit comes from the one with collisional velocity 1000 km/s; for operators with a linear dependence on transferred momentum, the two limits are about equal; for the operators with quadratic or cubic depedence on transferred momentum, the strongest limit comes from the source with collisonal velocity 4700 km/s.

4.3 Signal amplification

At last, I present the final and most significant result of this thesis: the possible amplification factor to the high-energy neutrino signal coming from WIMPs trapped within the Sun. The amplification factor, β, as described in section 3.4, is defined as the total flux of neutrinos relative to the same quantity when completely neglecting self-interaction.

Visualizations of parameter space with lines of constant β, for different WIMP masses and self-interaction operators, can be seen in figures 4.7–4.10. The horizontal axis is the WIMP-nuclei interaction strength, represented in terms of WIMP-nucleon (individual proton or neutron) constant cross-section, $\sigma_{\chi N}$. The WIMP-nucleon operator $\hat{\mathcal{O}}_1$ with isoscalar coupling is used for all figures and subfigures. The vertical axis is the WIMP self-interaction total cross-section, $\sigma_{\chi\chi}$. As most of the operators have a dependence on collisional velocity, the axis values are calculated under the assumption that this velocity is 1000 km/s.

The self-interaction operators that are represented in figures 4.7–4.10 are $\hat{\mathcal{O}}_1$, $\hat{\mathcal{O}}_7$, $\hat{\mathcal{O}}_3$, $\hat{\mathcal{O}}_{15}$, in that specific order. This way, they are presented in order of constant, linear, quadratic, and cubic dependence on transferred momentum. As demonstrated in figure 4.6, operators with the same dependence on transferred momentum have practically identical self-capture rates.

The excluded regions of the parameter space are represented by colour regions. The red colour region represent exclusions of the WIMP-nuclei cross-section, with limits provided by LUX [59]. The blue and green colour regions represent exclusions of the WIMP self-interaction strength, with limits from the Bullet Cluster [64] and dark matter halo simulations [9][10]. The origin of these limits are described in detail in section 3.3.

The light blue colour region represents the area of non-equilibration. It is the region of parameter space that does not produce a close-to-equilibrium amount of trapped WIMPs for the current age of the Sun, $t_\odot \simeq 4.5 \cdot 10^9$ years. The non-equilibrized region is defined to have neutrino signal strength that is less than 58 % of what if would be at equilibrium. The number 58 % is related to the fact that $\tanh^2(1) \simeq 0.58$. In the case of negligible self-interaction, the non-equilibrized region fulfills $\sqrt{C_s C_a} > t_\odot$.

The behaviour of the lines of constant β are very different in the equilibrium and non-equilibrium parts of parameter space. In the equilibrized region, the lines of constant β follow relation $\sigma_{\chi N} \propto \sigma^2_{\chi\chi}$. This is in good accordance with the equilibrium solution presented in equation (3.4.13). In the non-equilibrized area, the lines of constant β are independent of the WIMP-nucleon cross-section, $\sigma_{\chi N}$. This is in good accordance with the non-equilibrium solution presented in equation (3.4.16). In this case the annihilation rate, C_a, can be neglected and it turns out that the capture rate by nuclei, C_c, does not affect the relative signal amplification at all. However, it *does* affect the absolute signal and is still crucial for whether or not that signal is detectable.

All figures 4.7–4.10 assume the WIMP-nuclei interaction operator $\hat{\mathcal{O}}_1$ with isoscalar coupling, with its subsequent LUX limit for the different masses. The other WIMP-nuclei interaction operators have different capture rates at that limit, as illustrated by table 4.1. Because the total cross-section (evaluated at some collisional velocity) is directly proportional to the capture rate by nuclei, C_c, the lines of constant β and the equilibrium region have exactly the same shape. The only thing that differs between the different WIMP-nuclei operators is how much of the allowed parameter space is equilibrized. For the operator with the lowest maximum capture rate, $\hat{\mathcal{O}}_{11}$ with isovector coupling, the LUX limit completely excludes an equilibrized signal. For the operator with the highest maximum capture rate, $\hat{\mathcal{O}}_7$ with isoscalar coupling, the equilibrized part of the allowed parameter space is much wider. Other WIMP-nuclei operator do not allow for a higher signal amplification, since the highest β is found in the non-equilibrized region, where the capture rate by nuclei, C_c, is low.

For operators with no dependence on transferred momentum, $\hat{\mathcal{O}}_1$ and $\hat{\mathcal{O}}_4$, a signal amplification of several orders of magnitude is allowed, as is visible in figure 4.7. This is true also for operators with linear dependence on transferred momentum (i = 7,8,9,10,11,12), as visible in figure 4.8. In these cases it could be possible that self-interaction completely dominates the total capture of WIMPs by the Sun.

For the operators with quadratic dependence on transferred momentum (i = 3,5,6,13,14), the Bullet Cluster limit permits a smaller signal amplification, as visible in figure 4.9. In this case, WIMP capture by nuclei would be the dominant process.

For operator $\hat{\mathcal{O}}_{15}$, that has a cubic dependence on transferred momentum, the Bullet Cluster limit excludes any signal amplification larger than a few percent, as visible in figure 4.10. In this case, WIMP self-interaction has a negligable effect on the total capture rate.

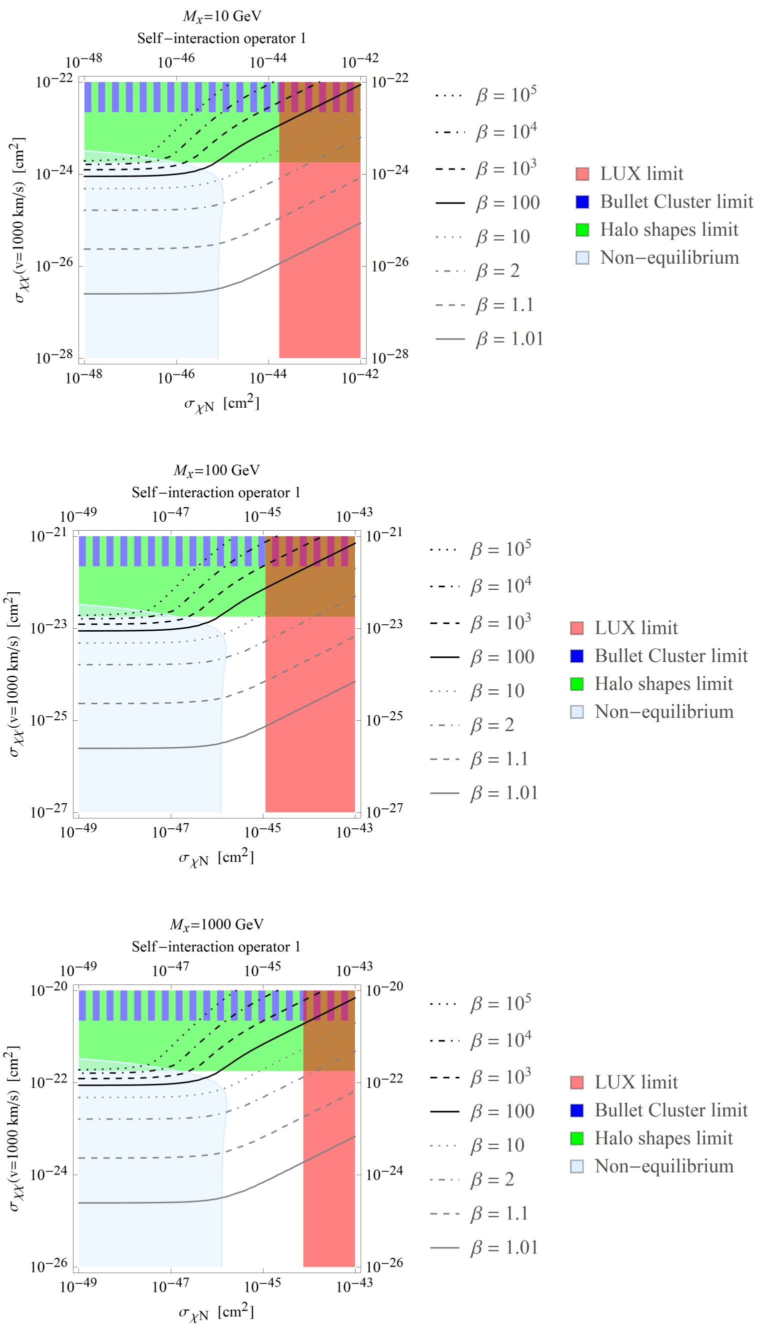

Figure 4.7: Lines of constant amplification, β, in the parameter space of WIMP-nucleon constant cross-section, $\sigma_{\chi N}$, and WIMP self-interaction cross-section, $\sigma_{\chi\chi}$, for self-interaction operator $\hat{\mathcal{O}}_1$ and different WIMP masses. The coloured regions represent parameter limits and area of non-equilibration.

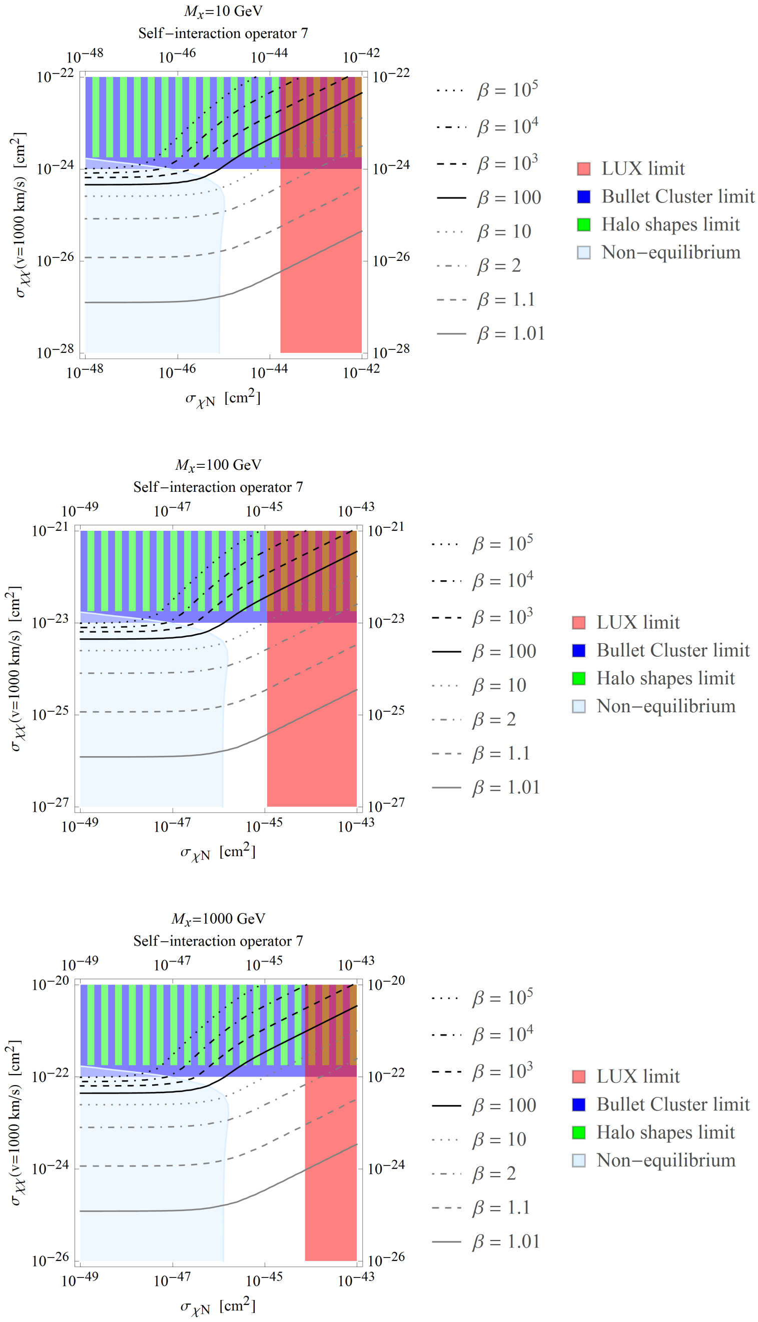

Figure 4.8: Lines of constant amplification, β, in the parameter space of WIMP-nucleon constant cross-section, $\sigma_{\chi N}$, and WIMP self-interaction cross-section, $\sigma_{\chi\chi}$, for self-interaction operator $\hat{\mathcal{O}}_7$ and different WIMP masses. The coloured regions represent parameter limits and area of non-equilibration.

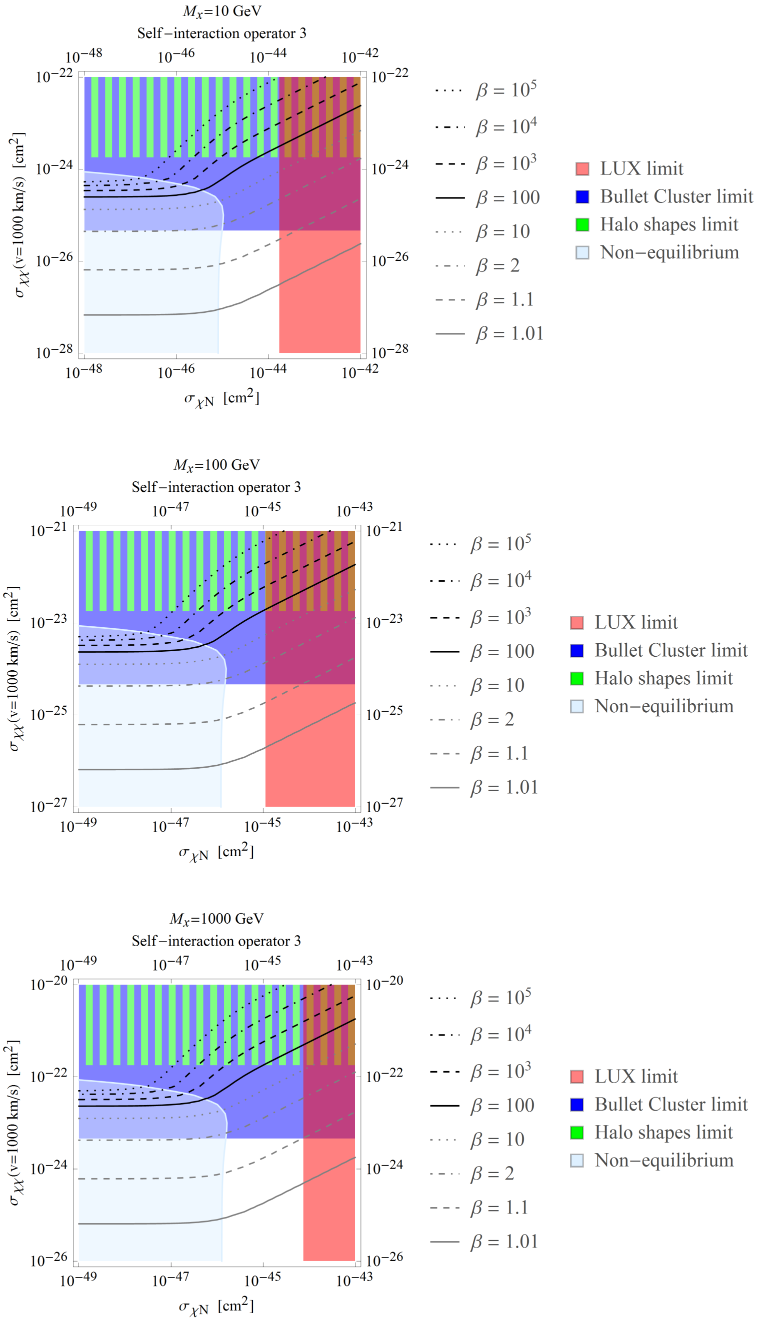

Figure 4.9: Lines of constant amplification, β, in the parameter space of WIMP-nucleon constant cross-section, $\sigma_{\chi N}$, and WIMP self-interaction cross-section, $\sigma_{\chi\chi}$, for self-interaction operator $\hat{\mathcal{O}}_3$ and different WIMP masses. The coloured regions represent parameter limits and area of non-equilibration.

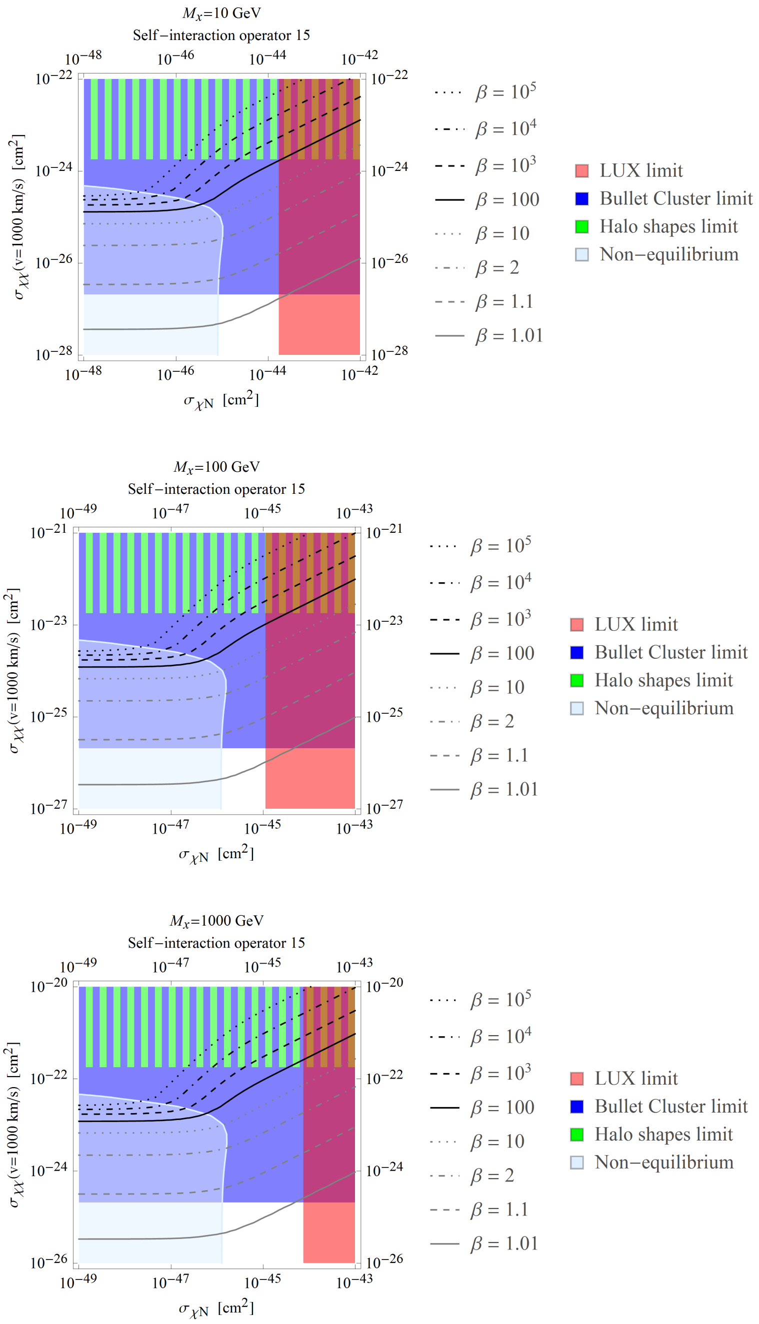

Figure 4.10: Lines of constant amplification, β, in the parameter space of WIMP-nucleon constant cross-section, $\sigma_{\chi N}$, and WIMP self-interaction cross-section, $\sigma_{\chi\chi}$, for self-interaction operator $\hat{\mathcal{O}}_{15}$ and different WIMP masses. The coloured regions represent parameter limits and area of non-equilibration.

5

Discussion

In this thesis I have explored the possibility that dark matter self-interaction has significant effect on the total dark matter capture rate of the Sun and, subsequently, that it also amplifies the neutrino signal coming from annihilation of captured dark matter particles in the Sun's core. By assuming that dark matter consists of Weakly Interacting Massive Particles (WIMPs) and utilizing an effective field theory in the non-relativistic regime, I have derived the capture rates and neutrino signal amplification factors. This has been done in the region of allowed parameter space, with exclusion limits from direct detection experiments [57] and galaxy cluster observation and simulation [9][10][64].

It has been found that a significant amplification to the neutrino signal at present time is possible; even an amplification of four orders of magnitude is not conclusively excluded. The largest amplifications are possible for WIMP self-interaction operators with constant or linear dependence on transferred momentum, as illustrated in figures 4.7 and 4.8. For WIMP self-interaction operators with quadratic dependence on transferred momentum, only an amplification less than a factor two is allowed, as illustrated in figure 4.9. In the case of cubic dependence on transferred momentum, amplifications of only a few percent is allowed, as illustrated in figure 4.10. The largest amplifications are found in the non-equilibrium region, which is the part of parameter space for which WIMP annihilation has not yet come into full effect at present time. Incidentally, this is also the region that gives off the weaker signal, so in terms of actual detection this is not preferred. However, even well into the equilibrium region, where the neutrino signal is strong, an amplification of at least one order of magnitude is possible within the current limits.

These results are contingent on some assumptions and approximations, some of which break down for very strong WIMP self-interaction and very weak WIMP-nuclei interaction. The assumptions that WIMPs quickly slow down and settle in the Sun's core and that they thermalize to core temperature are both compromised for the combination of very strong WIMP self-interaction and very weak WIMP-nuclei interaction. Exactly where this issue arises is not explored in detail in this thesis but the precise nature of the very high amplification factors ($\beta > 10^3$) should be taken with a grain of salt, especially far into the non-equilibrium region of parameter space. It is never-the-less valid that capture by self-interaction is the dominant process in those regions of parameter space.

The results of this thesis are novel and significant. The subject of WIMP capture by the Sun via self-interaction has previously only been explored in one article by Zentner [1]. In this article, a constant self-interaction cross-section is assumed, with roughly the same limit used in this thesis. It is found that significant amplification is only possible when the annihilation coefficient, $\langle \sigma_A v \rangle$, is at least one order of magnitude smaller than its expected value. This is in tension with the results of this thesis, as I find large amplification values for the expected value for the annihilation coefficient. Values in other regions of parameter space are in quite good accordance, as well the individual values for C_c, C_s, and C_a (capture rate by nuclei, capture rate by self-interaction, and annihilation rate). As seen in equation (3.4.12), that describes the amplification, the parameters C_c and C_a only occur as a product. This means that in terms of the signal amplification parameter, β, the effect of *increasing* the annihilation factor by one order of magnitude is nullified by *decreasing* the WIMP-nucleon cross-section by one order of magnitude. The results presented in the article by Zentner does not respect this analytical fact, as seen in the article's figure 2, panels (c) and (f).

The main result of this thesis is that self-interaction could significantly amplify the neutrino signal coming from WIMP annihilation within the Sun, even with the canonical value for WIMP annihilation and with current limits for WIMP interaction strengths. There are high hopes to finally detect these particles in the near future. Experiments are getting progressively bigger and more sensitive, both in the area of direct detection, such as the new XENON1T detector, and indirect detection, such as the PINGU extension to the IceCube detector. Perhaps a high-energy neutrino signal emanating from the Sun could be the "smoking gun" of dark matter particle detection. In this case dark matter self-interaction would be an important factor to consider.

Bibliography

[1] Zentner, A.R. (2009) *High-Energy Neutrinos From Dark Matter Particle Self-Capture Within the Sun. Phys.Rev.D*, volume 80, 063501.

[2] Wang, F., Wang, W., Yang, J.M. and Zhou, S. (2014) *Singlet Extension of the MSSM as a Solution to the Small Cosmological Scale Anomalies. Phys.Rev.D*, volume 90, 035028.

[3] Bertone, G., Hooper, D. and Silk, J. (2004) *Particle Dark Matter: Evidence, Candidates and Constraints. Phys.Rep.*, volume 405.

[4] Zwicky, F. (1933) *Die Rotverschiebung von extragalaktischen Nebeln. Helvetica Physica Acta*, volume 6, 110–127.

[5] Rubin, V., Ford, W. and Thonnard, N. (1980) *Rotational Properties of 21 SC Galaxies with a Large Range of Luminosities and Radii, from NGC 4605 to UGC 2885. ApJ*, volume 238, 471–487.

[6] Begeman, K.G., Broeils, A.H. and Sanders, R.H. (1991) *Extended Rotation Curves of Spiral Galaxies - Dark Haloes and Modified Dynamics. MNRAS*, volume 249, pp. 523–537.

[7] Dubinski, J. and Carlberg, R. (1991) *The Structure of Cold Dark Matter Halos. ApJ*, volume 378.

[8] Spergel, D.N. and Steinhardt, P.J. (2000) *Observational Evidence for Self-interacting Cold Dark Matter. Phys.Rev.Lett.*, volume 84:3760-3763.

[9] Rocha, M., Peter, A.H., Bullock, J.S., Kaplinghat, M., Garrison-Kimmel, S., Onorbe, J. and Moustakas, L.A. (2013) *Cosmological Simulations with Self-Interacting Dark Matter I: Constant Density Cores and Substructure. MNRAS*, volume 430.

[10] Zavala, J., Vogelsberger, M. and Walke, M. (2013) *Constraining Self-interacting Dark Matter with the Milky Way's Dwarf Spheroidals. MNRAS*, volume 431.

[11] Pontzen, A. and Governato, F. (2014) *Cold Dark Matter Heats Up. Nature*, volume 506.

[12] Mateo, M. (1998) *Dwarf Galaxies of the Local Group. Ann.Rev.Astron.Astrophys.*, volume 36, 435–506.

[13] Zaritsky, D., Smith, R., Frenk, C. and White, S. (1997) *Anisotropies in the distribution of satellite galaxies. ApJ*, volume 478.

[14] Hoekstra, H., Yee, H. and Gladders, M. (2002) *Anisotropies in the distribution of satellite galaxies. New Astron.Rev.*, volume 46, 767–781.

[15] Vikhlinin, A., Kravtsov, A., Forman, W., Jones, C., Markevitch, M., Murray, S.S. and Speybroeck, L.V. (2005) *Chandra Sample of Nearby Relaxed Galaxy Clusters: Mass, Gas Fraction, and Mass-Temperature Relation. ApJ*, volume 640, 691–709.

[16] Clowe, D., Gonzalez, A. and Markevitch, M. (2004) *Weak-Lensing Mass Reconstruction of the Interacting Cluster 1E 0657-558: Direct Evidence for the Existence of Dark Matter. ApJ*, volume 604, 596–603.

[17] Ade, P.A.R, et al. (2014) *Planck 2013 Results. I. Overview of Products and Scientific Results. A&A*, volume 571, A1.

[18] Adam, R., et al. (2015) *Planck 2015 results. I. Overview of products and scientific results.* European Space Agency.

[19] Bond, J., Efstathiou, G. and Silk, J. (1980) *Massive Neutrinos and the Large-Scale Structure of the Universe. Phys.Rev.Lett.*, volume 45.

[20] Dodelson, S. and Widrow, L.M. (1993) *Massive Neutrinos and the Large-Scale Structure of the Universe. Phys.Rev.Lett.*, volume 72.

[21] Rosenberg, L.J. and van Bibber, K.A. (2000) *Searches for invisible axions. Phys.Rept.*, volume 325, 1–39.

[22] Jungman, G., Kamionkowski, M., and Griest, K. (1995) *Supersymmetric Dark Matter. Phys.Rept.*, volume 267.

[23] Martin, S.P. (2016) *A Supersymmetry Primer.* Department of Physics, Northern Illinois University.

[24] Cheng, H.C., Feng, J.L. and Matchev, K.T. (2002) *Kaluza-Klein Dark Matter. Phys.Rev.Lett.*, volume 89.

[25] Greisen, K. (1966) *End to the Cosmic-Ray Spectrum? Phys.Rev.Lett.*, volume 16, 748–750.

[26] Ziaeepour, H. (2000) *A Decaying Ultra Heavy Dark Matter (WIMPZILLA): Review of Recent Progress. Grav.Cosmol.Suppl.*, volume 6, 128–133.

[27] Steigman, G., Dasgupta, B. and Beacom, J.F. (2012) *Precise Relic WIMP Abundance and its Impact on Searches for Dark Matter Annihilation. Phys.Rev.*, volume D86.

[28] Abercrombie, D., et al. (2015) *Dark Matter Benchmark Models for Early LHC Run-2 Searches: Report of the ATLAS/CMS Dark Matter Forum.* ATLAS-CMS Dark Matter Forum.

[29] Klasen, M., Pohl, M. and Sigl, G. (2015) *Indirect and Direct Search for Dark Matter. Prog.Part.Nucl.Phys.*, volume 85.

[30] Undagoitia, T.M. and Rauch, L. (2015) *Dark Matter Direct-Detection Experiments. J.Phys.G*, volume 43, 1.

[31] Akimov, D.Yu., et al. (2007) *The ZEPLIN-III dark matter detector: instrument design, manufacture and commissioning. Astropart.Phys.*, volume 27.

[32] Aprile, E., et al. (2016) *Physics reach of the XENON1T dark matter experiment. JCAP*, volume 027.

[33] Akerib, D.S., et al. (2013) *The Large Underground Xenon (LUX) Experiment. Nucl.Instr.Meth.Phys.Res.*, volume A704.

[34] Bernabei, R., et al. (2008) *The DAMA/LIBRA apparatus. Nucl.Instrum.Meth.*, volume A592, 297–315.

[35] Bernabei, R., et al. (2013) *Final model independent result of DAMA/LIBRA-phase1. Eur.Phys.J.*, volume C73.

[36] Kim, S.C., et al. (2012) *New Limits on Interactions between Weakly Interacting Massive Particles and Nucleons Obtained with CsI(Tl) Crystal Detectors. Phys.Rev.Lett.*, volume 108.

[37] Aalseth, C.E., et al. (2014) *Search for An Annual Modulation in Three Years of CoGeNT Dark Matter Detector Data.* CoGeNT Collaboration.

[38] Agnese, R., et al. (2013) *Demonstration of Surface Electron Rejection with Interleaved Germanium Detectors for Dark Matter Searches.* The SuperCDMS Collaboration.

[39] Armengaud, E., et al. (2011) *Final results of the EDELWEISS-II WIMP search using a 4-kg array of cryogenic germanium detectors with interleaved electrodes. Phys.Lett.*, volume B702.

[40] Behnke, E., et al. (2012) *First dark matter search results from a 4-kg CF_3I bubble chamber operated in a deep underground site. Phys.Rev.*, volume D86.

[41] Amole, C., et al. (2015) *Dark Matter Search Results from the PICO-2L C_3F_8 Bubble Chamber. Phys. Rev. Lett.*, volume 114.

[42] Felizardo, M., et al. (2013) *Final Analysis and Results of the Phase II SIMPLE Dark Matter Search. Phys.Rev.Lett.*, volume 108.

[43] Battat, J., et al. (2016) *First background-free limit from a directional dark matter experiment: results from a fully fiducialised DRIFT detector. Phys.Dark Univ.*, volume 9-10.

[44] Gaskins, J.M. (2016) *A Review of Indirect Searches for Particle Dark Matter. Contemp.Phys.*

[45] Hinton, J. (2004) *The Galactic sky through H.E.S.S. eyes. New Astron.Rev.*, volume 48, 331–337.

[46] Abeysekara, A.U., et al. (2014) *The Sensitivity of HAWC to High-Mass Dark Matter Annihilations. Phys.Rev.*, volume D90.

[47] Atwood, W.B., et al. (2009) *The Large Area Telescope on the Fermi Gamma-ray Space Telescope Mission. Astrophys.J.*, volume 697, 1071–1102.

[48] Picozza, P., et al. (2007) *PAMELA - A Payload for Antimatter Matter Exploration and Light-nuclei Astrophysics. Astropart.Phys.*, volume 27, 296–315.

[49] Battiston, R. (1998) *The Alpha Magnetic Spectrometer (AMS): search for antimatter and dark matter on the International Space Station. Nucl.Phys.Proc.Suppl.*, volume 65, 19–26.

[50] Achterberg, A., et al. (2006) *First Year Performance of The IceCube Neutrino Telescope. Astropart.Phys.*, volume 26, 155–173.

[51] Abbasi, R., et al. (2012) *The Design and Performance of IceCube DeepCore. Astropart.Phys.*, volume 35, 615–624.

[52] Aguilar, J.A., et al. (2011) *ANTARES: the first undersea neutrino telescope. Nucl.Instrum.Meth.*, volume A656, 11–38.

[53] Fukuda, Y., et al. (2003) *The Super-Kamiokande detector. Nucl.Instrum.Meth.*, volume A501, 418–462.

[54] Gould, A. (1987) *Resonant Enhancements in Weakly Interacting Massive Particle Capture by the Earth. The Astrophysical Journal*, volume 321, pp. 571–585.

[55] Bahcall, J.N., Pinsonneault, M.H. and Basu, S. (2001) *Solar Models: Current Epoch and Time Dependences, Neutrinos, and Helioseismological Properties. ApJ*, volume 555.

[56] Gondolo, P., Edsjo, J., Ullio, P., Bergstrom, L., Schelke, M. and Baltz, E. (2004) *DarkSUSY: Computing Supersymmetric Dark Matter Properties Numerically. JCAP*, volume 0407.

[57] Catena, R. (2015) *Dark Matter Signals at Neutrino Telescopes in Effective Theories. JCAP*, volume 1504.

[58] Anand, N., FitzPatrick, A.L. and Haxton, W. (2013) *Model-independent WIMP Scattering Responses and Event Rates: A Mathematica Package for Experimental Analysis. Phys.Rev.C*, volume 89.

[59] Catena, R. and Schwabe, B. (2015) *Form Factors for Dark Matter Capture by the Sun in Effective Theories. JCAP*, volume 1504.

[60] Ben Moore et al. (1999) *Dark Matter Substructure within Galactic Halos. ApJ*, volume 524.

[61] Kahlhoefer, F., Schmidt-Hoberg, K., Kummer, J. and Sarkar, S. (2015) *On the Interpretation of Dark Matter Self-interactions in Abell 3827. Mon.Not.Roy.Astron.Soc.*, volume 452.

[62] Miralda-Escudé, J. (2002) *A Test of the Collisional Dark Matter Hypothesis from Cluster Lensing. ApJ*, volume 564.

[63] Harvey, D., Massey, R., Kitching, T., Taylor, A. and Tittley, E. (2015) *The Non-Gravitational Interactions of Dark Matter in Colliding Galaxy Clusters. Science*, volume 347.

[64] Randall, S.W., Markevitch, M., Clowe, D., Gonzalez, A.H. and Bradac, M. (2008) *Constraints on the Self-Interaction Cross-Section of Dark Matter from Numerical Simulations of the Merging Galaxy Cluster 1E 0657-5. ApJ*, volume 679.